Light Water Reactor Sustainability Program

Inhomogeneous Aging of Nuclear Power Plant Electrical Cable Insulation

June 2021

PNNL-31443

Inhomogeneous Aging of Nuclear Power Plant Electrical Cable Insulation

Leonard S. Fifield, Witold Fuchs, Yelin Ni, Donghui Li, Madhusudhan R. Pallaka, Ana L. Arteaga, Mychal P. Spencer, and Andy Zwoster

June 2021

SUMMARY

Nuclear electrical cable insulation of the two most common types, ethylene-propylene rubber (EPR) and cross-linked polyethylene (XLPE), were subjected to thermal aging at temperatures like those used in historic environmental qualification. Materials were characterized using conventional tensile elongation at break (EAB) for both material types and indenter modulus for EPR. Cross-sections of the aged insulation were examined for evidence of inhomogeneous aging through the thickness of the material using nanoindentation, energy dispersive X-ray spectroscopy (EDS), and Fourier transform infrared spectroscopy (FTIR), as well as a new technique for tracking location specific aging—total color difference. We developed this fast and quantitative color analysis technique to identify diffusion limited oxidation (DLO) thresholds for cable insulation specimens and better address gaps in the literature. This work targeted three goals: first, to investigate whether DLO significantly affects lifetime prediction from cable qualification studies. Second, to identify the thresholds at which DLO occurs in three widely used nuclear power plant low voltage electrical cable insulations. Finally, to validate and demonstrate the developed color analysis technique for the identification of DLO in polymeric materials.

Cross-sections from each cable material—Anaconda EPR, Rockbestos XLPE, and Brand-Rex XLPE—at each aging temperature and duration were imaged and analyzed for total color difference versus that of the as-received materials. Overall color change was observed to track with exposure severity. Inhomogeneous color change, manifesting as increased change near the inner and outer edges of the insulation, was observed. The inhomogeneous aging behavior was seen to vary among the three materials, being most prominent and temperature-dependent in the Anaconda EPR, present at all temperatures but mainly edge restricted in the Rockbestos XLPE, and not evident in the Brand-Rex XLPE. Oxidation was confirmed as the source of the outer edge inhomogeneous color change using nanoindentation, EDS and FTIR. Aging at the interior edge of the insulation was also seen to be material dependent, being greatest in the Anaconda EPR, less evident in Rockbestos XLPE, and not evident in the Brand-Rex XLPE. The exterior inhomogeneous oxidation behavior is understood to result from classic DLO, but the interior accelerated degradation is thought to be due to contact with the conductor leading to copper-ion catalyzed oxidation.
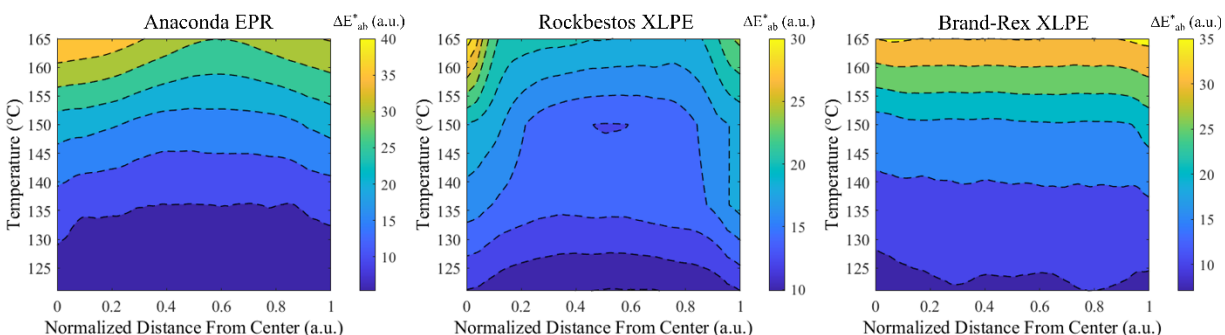
Total color difference (ΔE^*_{ab}) variations with increasing temperature for the three materials explored at an exposure of approximately 30 days. DLO is indicated by curvature of the contour lines (---). A normalized distance of 0 is the edge next to the conductor and a distance of 1 is the external edge.

Activation energy (E_a) values were calculated for the three materials using EAB, which is thought to be insensitive to DLO. E_a values were also calculated from the average total color difference (ΔE^*_{ab}) of each material, data that was observed to be affected by the DLO. It was found that the E_a calculated from ΔE^*_{ab} for Anaconda EPR, for which DLO was strongly observed, was slightly higher than the E_a calculated from EAB. That is, the EAB prediction for E_a was slightly more conservative: 19% lower E_a for EAB than for ΔE^*_{ab}, plus/minus 14% for Anaconda EPR. For the Rockbestos XLPE, in which DLO was observed at all temperatures considered, the EAB-derived E_a was found to be higher by 40% plus/minus 15%. For the Brand-Rex XLPE material considered, in which no DLO was observed, the EAB- and ΔE^*_{ab}-derived E_a values were found to be very similar, 17% plus/minus 15% greater for ΔE^*_{ab}.

Activation energy value ranges for the three materials explored using elongation at break (EAB) and total color change (ΔE^*_{ab}) at an endpoint of 50% EAB retention. Previous work has indicated EAB is not sensitive to diffusion limited oxidation (DLO), while this work has demonstrated that is ΔE^*_{ab} is sensitive to DLO.

Material	EAB-Derived E_a (kJ/mol)	ΔE^*_{ab}-Derived E_a (kJ/mol)	Observed DLO Trends
Anaconda EPR	105 to 119	119 to 157	Time and temperature dependent
Rockbestos XLPE	100 to 119	66 to 90	Edge restricted
Brand-Rex XLPE	88 to 115	103 to 139	Not evident

DLO was found to affect calculated E_a values by a degree that differed by material. Uncertainty in the values calculated led to similar results between metrics thought to be DLO-affected and not to be DLO-affected. Total color change was determined to be a useful and effective way to quantify location-specific aging; a method that is both quick and convenient. The conclusions that can be drawn from this work are limited by the materials and conditions (temperatures) explored, but also by the state of the material available (levels of service aging, material thickness, material shape). It appeared evident, especially in the Anaconda EPR, that the materials in contact with the insulation during service strongly affected the material aging (such as copper-catalyzed oxidation). Further research to understand the impact of inhomogeneous aging on cable aging management would benefit from application of the techniques developed in this work to 1) additional cable materials (formulation, manufacturers), 2) insulation samples of various thicknesses available in sufficient quantity and form (pressed mats of uniform thickness) for oxygen permeation testing, and 3) investigation of cable inhomogeneous aging of non-DLO origin such as copper-catalyzed oxidation and diffusion of chloride, antimony and other species from flame retardant jacket materials.

ACKNOWLEDGEMENTS

CONTENTS

FIGURES

TABLES

ACRONYMS

BAS	basic auto-oxidation scheme
CI	carbonyl index
CIE	Commission on Illumination
CSPE	chlorosulfonated polyethylene
DLO	diffusion limited oxidation
ΔE^*_{ab}	total color difference
E_a	activation energy
EAB	elongation at break
EDS	energy-dispersive X-ray spectroscopy
EPR	ethylene-propylene rubber
EMDA	Expanded Materials Degradation Assessment [1]
EPDM	ethylene-propylene-diene elastomer
EPRI	Electric Power Research Institute
ETFE	ethylene-tetrafluoroethylene
FTIR	Fourier-transform infrared spectroscopy
IEC	International Electrotechnical Commission
IEEE	Institute of Electrical and Electronics Engineers
IPAM	Indenter Polymer Aging Monitor
ISO	International Standards Organization
LWRS	Light Water Reactor Sustainability
NPP	nuclear power plant
NIH	National Institute of Health
PDE	partial differential equation
PE	Polyethylene
PNNL	Pacific Northwest National Laboratory
PVC	polyvinyl chloride
rEAB	EAB retention (fraction of initial EAB)
ROI	region of interest
SLR	subsequent license renewal
SR	silicone rubber
sRGB	standard red-green-blue
UTS	ultimate tensile strength
XLPE	cross-linked polyethylene

1. INTRODUCTION

Approximately 20% of the electricity produced in the United States comes from nuclear power plants (NPPs) [2]. Originally, NPPs were qualified for an operational lifetime of 40 years [3,4]. As described in the foreword of the U.S. Nuclear Regulatory Commission's (NRC's) Expanded Materials Degradation Assessment (EMDA) Volume 5: Aging of Cables and Cable Systems [5], and according to Title 10 of the Code of Federal Regulations, Part 54 (10 CFR 54), "Requirements for Renewal of Operating Licenses for Nuclear Power Plants", NPPs can apply for 20-year license extensions following the original 40-year operating period. While most NPPs have entered extended license periods to 60 years, some are considering license extension to 80 years of operation [6]. The viability of a subsequent license renewal (SLR) is dependent upon the NPPs operating safely in accordance with the licensing basis established with the original 40-year license. Hence, the NRC has developed aging management program requirements to promote the safe operation of NPPs over license extension periods. The EMDA report identified cable aging-related issues that may be important for the SLR of NPPs.

Based on the issues raised in EMDA Volume 5, a U.S. Department of Energy-sponsored research and development roadmap workshop report [7], and additional emerging issues, Pacific Northwest National Laboratory (PNNL) prioritized a list of 11 cable-aging knowledge gaps focusing on the degradation of cable insulation [8]. From this list, four knowledge gaps were selected for investigation as described by Fifield et al. [8], including: (1) diffusion limited oxidation (DLO) effects due to oxygen permeability hindrance at the polymer surface during accelerated aging [9,10], (2) dose-rate effects where polymer degradation is not only a function of total absorbed gamma dose, but also of the dose rate [11], (3) inverse temperature effects in which degradation due to gamma irradiation is higher at lower temperatures [12], and (4) synergistic effects due to the combined interactions between temperature and radiation [13,14]. Of these four cable knowledge gaps, the focus of this report is on inhomogeneous aging as it relates to DLO.

Historically, manufacturers qualified electrical cables for 40-year operational lifetime using accelerated aging at temperatures and gamma radiation dose rates well above those experienced by cables in service [15]. Previous work identified highly elevated accelerated aging conditions as producing so-called DLO in polymers due to oxidation rates being greater than oxygen diffusion rates into the material from the surrounding atmosphere [9]. In such a situation, the concentration of dissolved oxygen within the material, and away from the atmospherically exposed surfaces, can drop to zero, inhibiting thermo-oxidative degradation of the interior material and leading to inhomogeneous aging of the insulation. Through this phenomenon, DLO may lead to overestimation of the operational lifetime of electrical cable components qualified using highly elevated accelerated aging conditions as DLO is not expected to occur in these components under normal NPP operating conditions [16]. Uncertainties still exist regarding the impact of DLO on NPP electrical cable qualification, such as the threshold temperatures and exposure durations beyond which DLO is prevalent and how these thresholds compare to conditions employed during historical cable qualification [17]. To support SLR of NPPs to 80-years or more, additional information regarding the impact of DLO on the historical qualification of electrical cables is needed.

In this study, two common nuclear cable insulation materials [3]— ethylene-propylene-rubber (EPR) and cross-linked polyethylene (XLPE)—were aged at four temperatures (121°C, 136°C, 150°C, and 165°C) for select exposure durations to determine DLO threshold conditions and the impact of DLO on cable thermo-oxidative reaction activation energy (E_a) values. First, in Section 2, the two cable insulation material types investigated are described. Then, in Section 3, accelerated aging involving elevated temperature applied to the insulation specimens is discussed. In Section 4, the characterization techniques used to perform this work are described. These include elongation at break (EAB), total color difference, reduced elastic modulus, carbonyl index (CI), and oxygen content as measured by energy dispersive X-ray spectroscopy (EDS). Section 5 discusses theory of polymer degradation and a model for DLO. Characterization results are provided in Section 6, followed by a discussion of results in Section 7. Finally, concluding remarks are made in Section 8.

2. MATERIALS

The materials investigated were selected from those commonly found within nuclear containment to enhance the relevancy of this work. Both EPR and XLPE were selected for analysis of DLO effects because insulation material types like these are present within at least 75% of nuclear containments in U.S. NPPs, as shown in Table 1. In addition to the selected material types, low-voltage nuclear grade instrumentation cables were selected because approximately 81% of electrical cables within U.S. NPPs are low-voltage instrument and control cables [18]. Furthermore, the investigated materials were extracted from cables produced by the most common manufactures of electrical cables for NPPs as shown in Table 1 and Table 2. The as-received electrical cables of this report were harvested from the decommissioned Crystal River Unit 3, an activity coordinated by the Electric Power Research Institute (EPRI). As such, the selected materials have previous aging history that is not accounted for in the analyses of this report (see Table 3).

Table 1. Most common nuclear cable insulation material types in containment (left) and a sort of the most common manufacturers' insulations within NPPs (right). (Percent of units indicated are approximate values.)

Insulation	Percent of Units (%) [19,20]	Manufacturer	Insulation	Number of Plants [19,20]
XLPE	90	Rockbestos	Firewall III XLPE	61
EPR/EPDM	75	Anaconda	EPR	35
SR	27	Brand-Rex	XLPE	30
CSPE	24	Okonite	EPR	26
ETFE	15	Kerite	HTK	25
PVC	7	Rockbestos	Coaxial XLPE	24
PE	3	Raychem	XLPE	23
Neoprene	3	Samuel Moore	EPR	19
Polyimide	3	BIW	Bostrad 7E EPR	19
Polyalkene	2	Kerite	Flame Retardant EPR	13

XLPE = cross-linked polyethylene; EPDM = ethylene-propylene-diene elastomer; EPR = ethylene-propylene rubber; SR = silicone rubber; CSPE = chlorosulfonated polyethylene; ETFE = ethylene tetrafluoroethylene; PVC = polyvinyl chloride; PE = polyethylene; HTK = high-temperature Kerite.

Table 2. Nuclear grade instrumentation cables used in this report.

Manufacturer	Jacket Labeling	Jacket Material	Insulation Material
Anaconda	Anaconda-Y 4/C #16 Flame-Guard FR-EP 600 V	CPE	EPR
Rockbestos	2/C 16 A-WG Rockbestos® 600 V B/M NO. NK-35A	CSPE	XLPE
Brand-Rex	BRAND-REX Ultrol 600 V 1 Shielded PR #16 AWG	CSPE	XLPE

CSPE = chlorosulfonated polyethylene; XLPE = cross-linked polyethylene; EPR = ethylene-propylene rubber; CPE = chlorinated polyethylene.

Table 3. Aging history of the Crystal River Unit 3 harvested electrical cables of this report.

Identifier	Manufacture Date	Installation Date	Location	Years in Service
Anaconda EPR	February 1985	April 1985	Reactor Coolant	30
Rockbestos XLPE	February 1993	March 1994	Industrial Cooling	21
Brand Rex XLPE	April 1986	September 1994	Main Feedwater	21

2.1   Components of As-Received Electrical Cables

Components of the low-voltage nuclear grade instrumentation cables of this report are shown in Figure 1. The white insulated conductors were extracted from the electrical instrumentation cables of Table 2 by first carefully removing the chlorinated polyethylene (CPE, Anaconda EPR insulation) or chlorosulfonated polyethylene (CSPE, Rockbestos XLPE and 2 insulations) jackets. A wire stripping tool was then used to score the insulation in 100 mm increments. Afterwards, the exposed conductors were fixed in place with a vice and the insulation removed by gently pulling the insulation from over the conductors. The extracted insulation specimens were 100 mm in length. The tubular cross-sections of the insulation specimens were measured as 5.77 mm^2 (2.81 mm outer diameter), 5.07 mm^2 (2.78 mm outer diameter), and 4.80 mm^2 (2.81 mm outer diameter) for the Anaconda EPR, Rockbestos XLPE, and Brand Rex XLPE insulations, respectively.

2.2   Spectra of Extracted Insulation Specimens

The material types of the extracted insulation were confirmed by comparing their absorbance spectra to literature data using Fourier-transform infrared spectroscopy (FTIR). The spectra of the as-received insulation specimens are shown in Figure 2. Due to their chemical structure, methylene absorption (-CH$_2$-) is useful for identification of both EPR and XLPE. For both material types, strong characteristic methylene asymmetric and symmetric stretching absorbance peaks were measured at 2916 cm^{-1} and 2848 cm^{-1}, respectively [21,22]. In addition, both material types demonstrate characteristic methylene bending modes at 1462 cm^{-1} (scissoring), 1349 cm^{-1} (wagging), and 729 cm^{-1} (rocking), analogous to those reported in literature [23–25]. All three insulation materials exhibited carbonyl bonds in the range of 1650 to 1750 cm^{-1}, likely due to oxidation during service employment or due to the presence of antioxidants within the supplied materials.
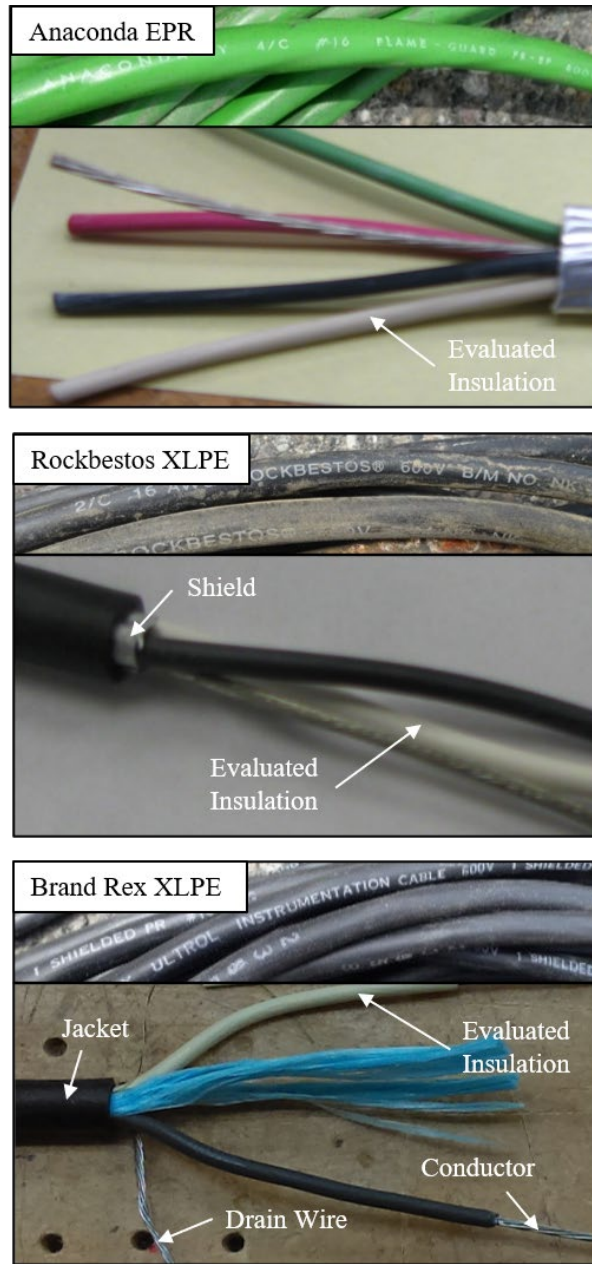
Figure 1. The as-received nuclear grade electrical cables and their exposed components. The evaluated white insulations selected for analysis are indicated in the figure.

a)
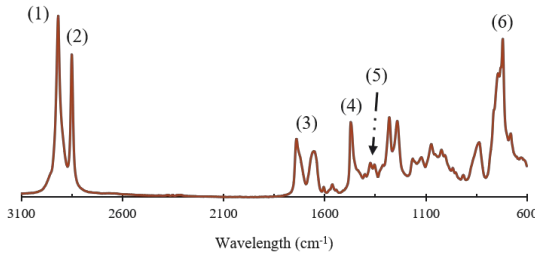
Location	K (cm⁻¹)	Functional Groups
(1)	2916	CH_2 asymmetric stretch
(2)	2848	CH_2 symmetric stretch
(3)	1650-1750	carbonyl (C=O) stretch
(4)	1462	CH_2 scissoring
(5)	1349	CH_2 wagging
(6)	729	CH_2 rocking

b)
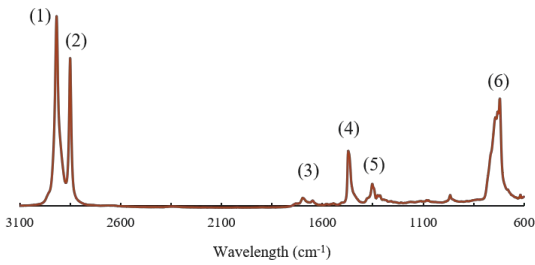
c)
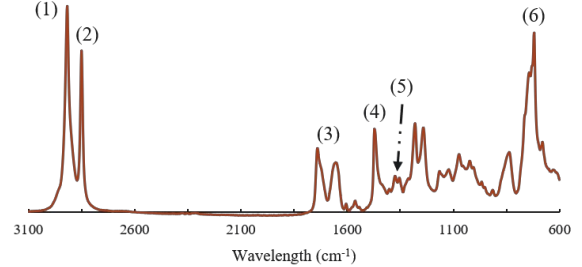
Figure 2. FTIR absorbance spectra of as-received low-voltage nuclear grade cable insulations a) Anaconda EPR, b) Rockbestos XLPE and c) Brand Rex XLPE.

3. THERMAL AGING

Insulation specimens were attached to alligator clips labeled with unique specimen identifiers. The specimens were hung from a rack in an oven (Thermo Scientific Heratherm OMH180) similar to the oven shown in Figure 3 and exposed to one of the conditions shown in Table 4. To evaluate the effects of DLO, temperatures were selected based on historical NPP cable insulation qualification analyses and previously published work to bracket the temperature range where DLO was expected to occur [17]. Oven temperature was controlled through integrated thermocouple feedback and adequate air circulation was ensured to minimize artifacts associated with local oxygen depletion surrounding the specimens during aging.

Figure 3. Clipped insulation specimens in an air-circulating oven.

Table 4. Evaluated test conditions for exposure of nuclear grade EPR and XLPE cable insulation specimens.

T (°C)	Exposure (Days)	T (°C)	Exposure (Days)	T (°C)	Exposure (Days)	T (°C)	Exposure (Days)
121	29	136	10	150	10	165	1
121	84	136	20	150	20	165	6
121	142	136	30	150	30	165	12
121	197	136	41	150	40	165	18
121	252	136	62	150	50	165	24
121	280	136	80	150	60	165	30

4.   EXPERIMENTAL METHODS

To investigate the onset of DLO for the investigated material types, six characterization methods were employed as discussed below.

4.1   Elongation at Break Measurement Using a Tensile Machine

Following IEC/IEEE 62582-3, tensile EAB was measured for as-received and aged insulation specimens [26]. Table 5 lists the test parameters for both material types. For each aging condition, the insulation specimens were cut to a length of 45 mm and the inner and outer diameters were measured using a digital caliper. A black permanent marker with a fine tip size was used to draw two gauge marks centered and at 20 mm separation on the insulation specimens. Afterwards, the insulation specimens were conditioned following ASTM D618 Procedure A: at least 40 hours at $23°C \pm 2°C$ and $50\% \pm 10\%$ relative humidity [27]. Humidity was controlled by placing the specimens in a covered desiccator charged with a saturated solution of potassium carbonate and deionized water (fixed humidity point of 43% [28]). A data logger was placed in the desiccator to monitor both temperature and humidity. After conditioning, end tabs of 5 mm length were placed over the ends of specimens with an approximate gap of 2 mm between the ends of specimens and the end tabs (see Figure 4). The method of attachment of the end tabs to the specimen depended upon the material type: two layers of tissue (Kimtech Science) were placed between the specimen and end tabs to avoid slippage of the end tabs on the EPR specimens, and the end tabs were gently compressed prior to placement on the XLPE specimens. After attachment of the end tabs, the specimens were placed centered and along the axis of a pair of pneumatic grips at a separation of 30 mm. A testing rate lower than that specified in IEC/IEEE 62582-3 was used to minimize early failure of specimens. As shown in Figure 4, a tensile testing machine (Instron® 3360 Universal Testing System, Norwood, MA) was used to apply tension to the specimens. Load versus displacement curves were generated for each insulation specimen and final elongation measured was used to calculate EAB, the difference between the final length and the initial length divided by the initial length. For each aging condition, EAB was calculated for three insulation specimens and the average value reported. Samples that experienced premature failure (as observed by failure in the grip before tension was applied) were removed from the data set, resulting in some specimens having fewer data points and. Data from extremely aged samples, with EAB approximately equal to zero, were deemed not constructive for the analyses and were not included in analyzed datasets for EAB or the other analytical techniques. In addition to EAB, tensile strength was calculated for each insulation specimen as the maximum measured load divided by the cross-sectional area (as measured by ImageJ (NIH) using images collected for color analysis).

Table 5. Test parameters utilized for EAB measurements.

Material Type	Test Rate (mm/min)	End Tab Material	Grip Pressure (psi)
EPR	20	CSPE (RSCC, I46-0021 Jacket)	50
XLPE	10	XLPE (Grainger, 10A671)	60

CSPE = chlorosulfonated polyethylene; EPDM = ethylene-propylene-diene elastomer; XLPE = cross-linked polyethylene.
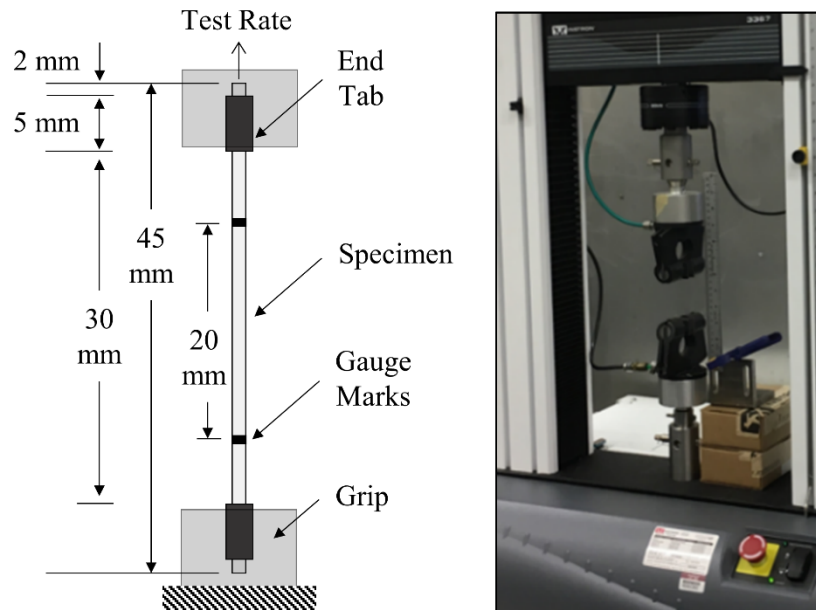
Figure 4. (Left) testing schematic for tensile testing of the insulation specimens and (right) digital image of the test frame.

4.2 Total Color Difference Measurement Using a Digital Camera

Polymeric specimens darken upon aging when exposed to thermal stress. Following ASTM D1729 and ASTM D2244, the total color difference (ΔE^*_{ab}) of the aged with respect to the as-received insulation specimens was measured using a light booth (GTI MiniMatcher MM 2e) and digital camera (Nikon D5300) [29,30]. Prior to color measurement, tubular insulation specimens were first cut to a thickness between 0.5 to 1.0 mm to enable imaging of their cross-sections. Next, the exposed cross-sectional surfaces were polished using a combination of liquid nitrogen and a successive series of sandpaper grits from 800 to 2500 (approximately 8.4 ± 0.5 μm final surface roughness) to remove surface defects generated during cutting. A clamp was then used to fix the digital camera in place and orient the camera lens perpendicular to the display plane of the light booth. To optimize the quality of the collected images, the digital camera settings used were as follows: an exposure time of 1/3 s to enhance color saturation, an aperture of f14 to enhance depth of field, and an ISO setting of 100 to reduce background noise. A wireless remote control (Nikon ML-L3) was used to ensure the camera did not move during image collection and to facilitate batch processing. In the light booth, a standard International Commission on Illumination (CIE) D65 light was used and background lighting in the room was extinguished during image collection. To facilitate image calibration and conversion to the CIE XYZ color space (and subsequently the L*a*b* color space [defined below]), a color reference target was first placed on the light booth display plane and an image captured. Next, the color reference target was removed, and the polished insulation specimens were placed on the
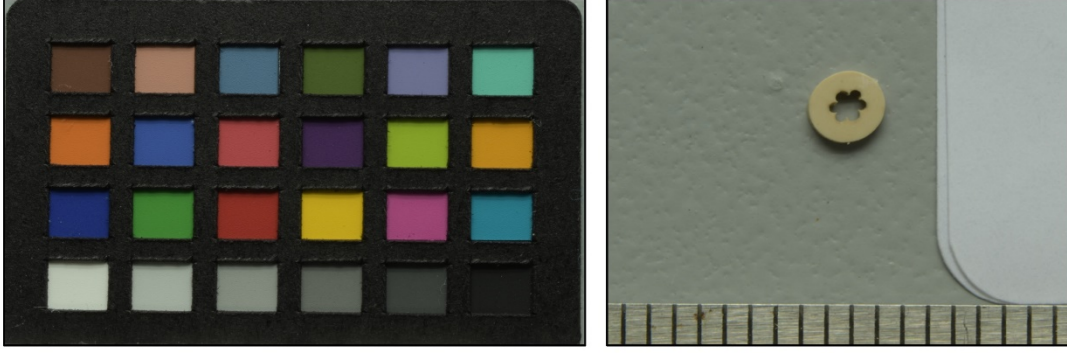
Figure 5. (Left) color reference target used to convert (right) input color image to a multi-spectral calibrated image.

display plane next to a reference scale as shown in Figure 5. One image was then collected for each aging condition.

Due to their inherent components and internal processing, a digital camera and lens will modify the color in digital images; therefore, it is necessary to map these modified colors into a system with an absolute measure of color prior to quantifying color changes in specimens tested. This process is summarized and visualized in Figure 6. ImageJ (NIH) was used in conjunction with the micaToolbox [31,32] to convert the collected image values to CIE XYZ color space. First, the six grey standards located on the bottom row of the color reference target (see Figure 5) were converted to reflectance values using manufacturer-supplied standard Red Green Blue (sRGB) triplets for each grey standard and then using an iterative least log slope approach [33] to convert the triplets to reflectance values. Second, the grey reflectance values were used to create a linear normalized reflectance stack, or calibrated multispectral image, for each collected image. Third, a cone-catch model [32] was generated based upon the charted reflectance spectra of the color reference target. Fourth, the cone-catch model was used to map the linear normalized reflectance stack to the CIE XYZ color space. Lastly, the measured XYZ color space values were mapped to D65 reference white point CIE L*a*b* color space through the built-in MATLAB$^{®}$ function *xyz2lab*. The total color difference calculation is shown in Equation (1), where $L*_S$, $a*_S$, and $b*_S$ are the reference L*a*b* values and $L*_B$, $a*_B$, and $b*_B$ are the specimen L*a*b* values. The mean L*a*b values of the as-received specimens were selected as reference values. The total color difference was measured for each pixel in the captured images and a surface profile was generated for each test condition. For each surface profile, total color difference was mapped and averaged across twelve locations as shown in Figure 6 to quantify DLO.

$$\Delta E_{ab}^* = \sqrt{(\Delta L^*)^2 + (\Delta a^*)^2 + (\Delta b^*)^2} \tag{1}$$

$$\Delta L^* = L_B^* - L_S^*$$

$$\Delta a^* = a_B^* - a_S^*$$

$$\Delta b^* = b_B^* - b_S^*$$
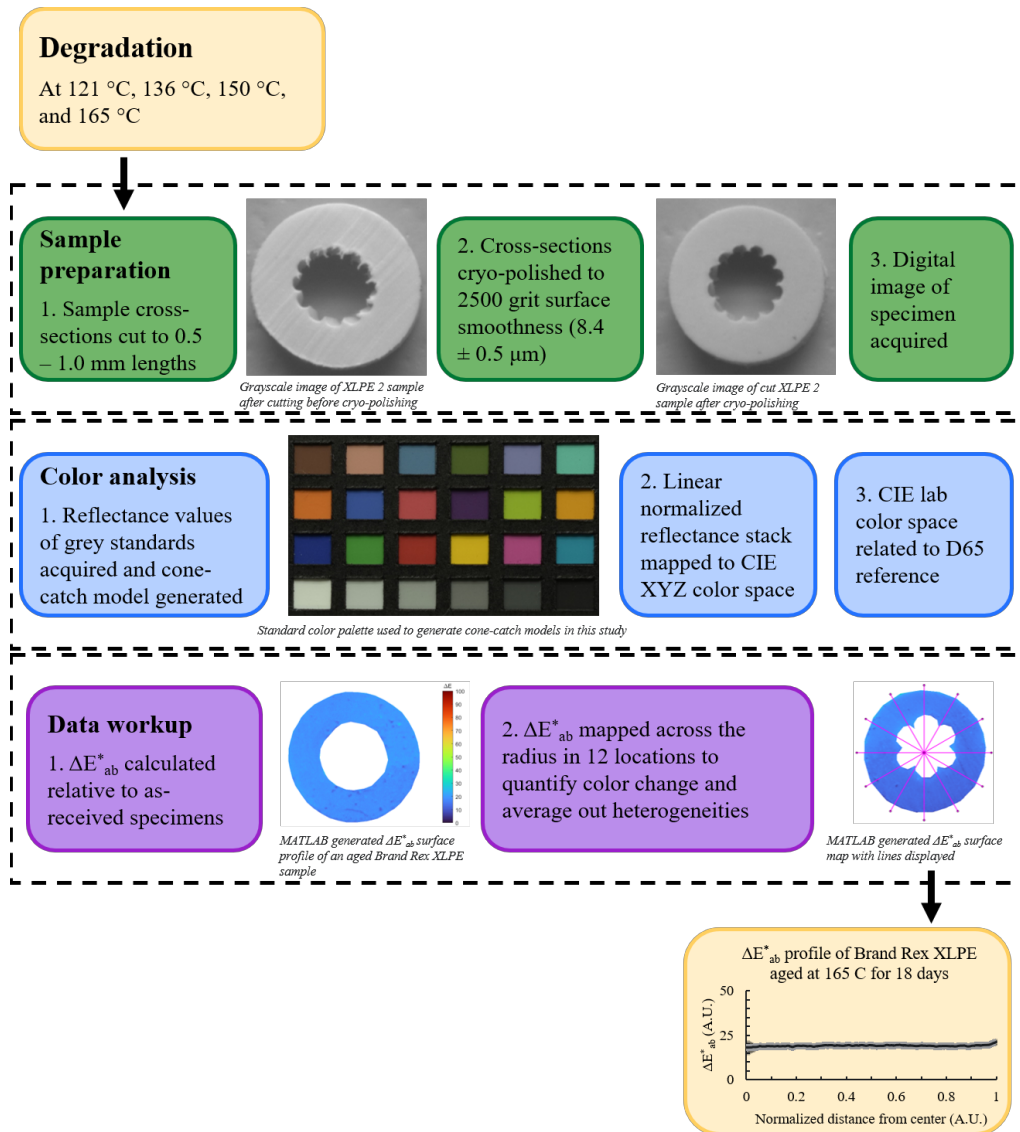
Figure 6. Process for analyzing the insulation specimens using total color difference.

4.3 Modulus and Hardness Measurement Using Nanoindentation

The modulus and hardness of the aged insulation specimens were measured using nanoindentation to validate total color difference as a metric to quantify DLO. Exemplary test conditions for Anaconda EPR were selected for comparison as shown in Table 6. The insulation specimens were first cut to lengths of approximately 5 mm. Next, the specimens were embedded into epoxy and their cross-sections prepared with polishing equipment (Struers Tegramin-30) using the following steps:

1. Plane ground on silicon carbide paper up to 1200 grit using water as a lubricant

2. Polished at a load of 25 N for 10 min using 3 μm alumina suspension (150 RPM)

3. Polished at a load of 20 N for 5 to 10 min using 1 μm alumina suspension (150 RPM)

4. Polished at a load of 15 N for 5 to 10 min using 0.05 μm alumina suspension (150 RPM).

Table 6. Test conditions selected to evaluate total color difference as metric for DLO.

T (°C)	Exposure (Days)
As-received	-
121	29
165	1
165	16

Specimens were cleaned with soap and water, rinsed with ethanol, and dried in air between each polishing step. After polishing, modulus and hardness of embedded specimen cross-sections were measured using a nanoindenter (Nanovea PB1000, see Figure 7) equipped with a Berkovich tip. The indenter was first calibrated by indenting on a fused quartz calibrant with known material properties. Specimens were then indented at a rate of 40 mN/min to a maximum force of 20 mN, followed by unloading at a rate of 40 mN/min. A total of 10 indentations were made on the cross-section of each specimen with a spacing of 80 µm spanning from the outside to inside edges of the insulation cross-section. An example of the indentation locations is shown in Figure 7. The (reduced) elastic modulus and hardness were calculated using the supplied nanoindentation software and are given by Equations (2) and (3), respectively, where P_{max} is the maximum loading, A is the estimated contact area, dP/dh is the slope of the initial portion of the unloading curve, and δ is a factor associated with the probe tip ($\delta = 1.034$ for Berkovich).

$$E = \left(\frac{dP}{dh}\right)\frac{\sqrt{\pi}}{2}\frac{1}{\sqrt{A}}\frac{1}{\delta} \tag{2}$$

$$H = \frac{P_{max}}{A} \tag{3}$$
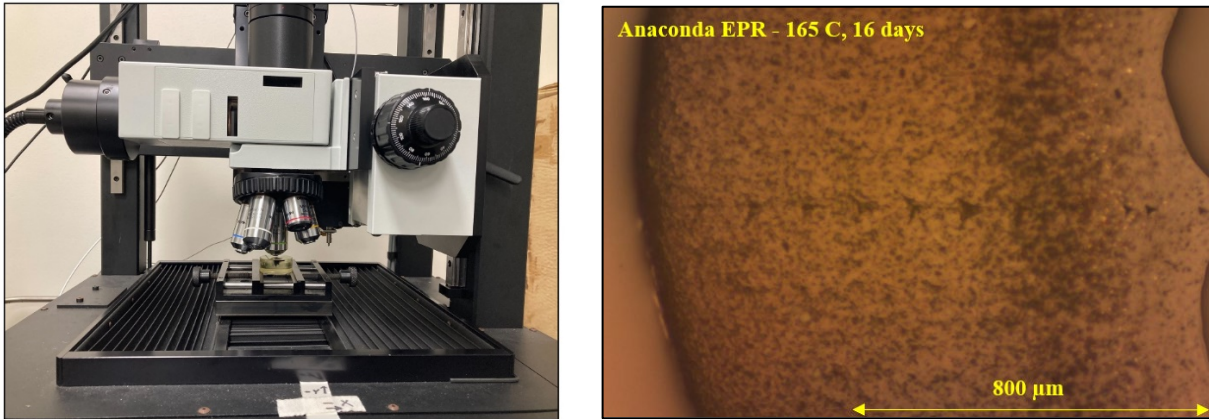
Figure 7. (Left) digital image of the nanoindenter used in this study and (right) image of cable insulation specimen during analysis displaying visible indents.

4.4   Carbonyl Index Measurement Using Microscope FTIR

Microscope FTIR attenuated total reflectance (ATR) (Bruker Lumos) was used to measure the carbonyl index of the insulation specimen cross-sections for comparison to and validation of total color difference. Exemplary test conditions for Anaconda EPR were selected for comparison. Insulation specimens were first cut to a thickness between 0.5 to 1.0 mm to enable imaging of their cross-sections. Next, exposed cross-sectional surfaces were polished using a combination of liquid nitrogen and 2500 grit sandpaper (approximately 8.5 ± 0.5 µm surface roughness) to remove surface defects generated during cutting. The
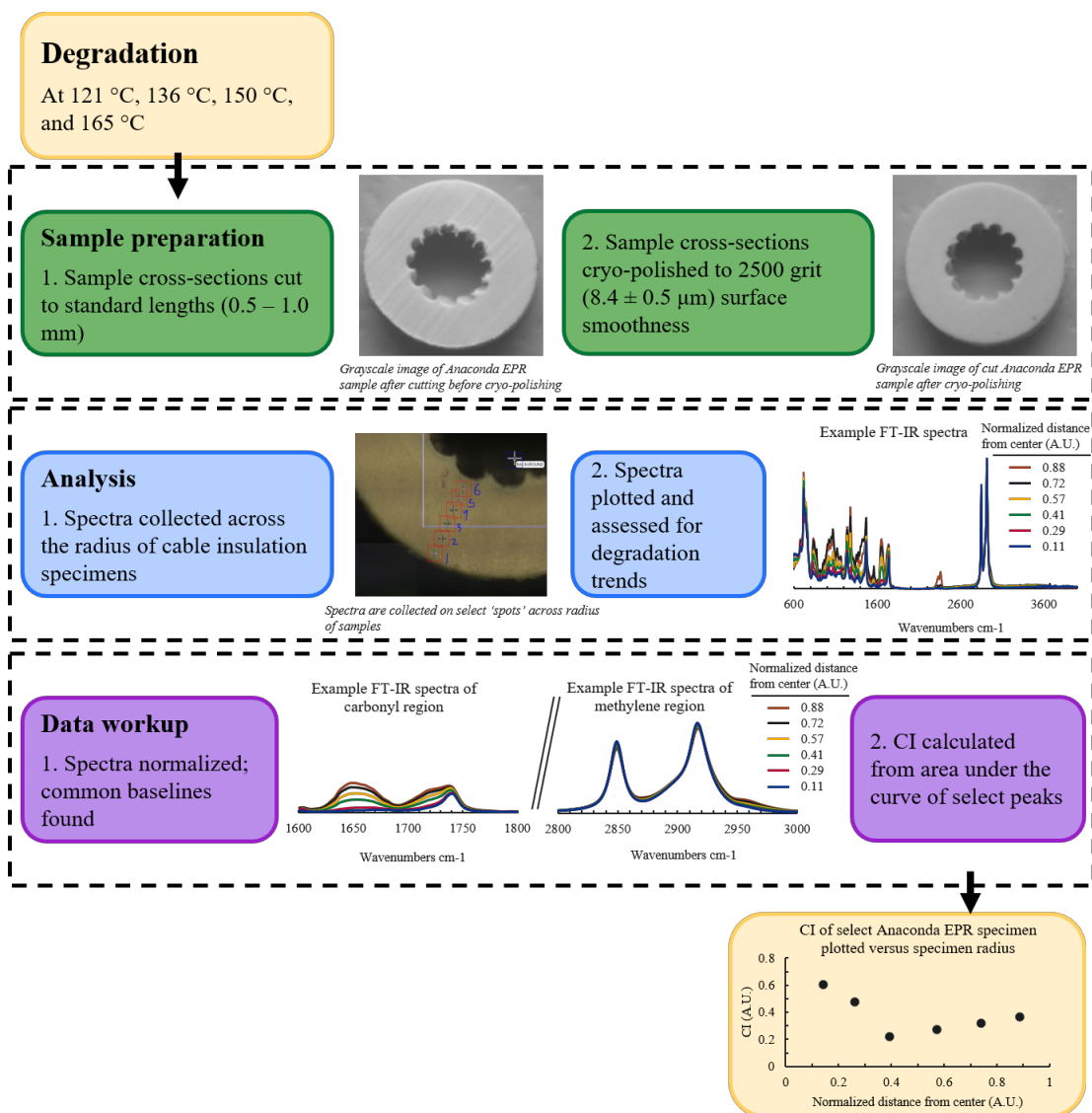
Figure 8. Process for analyzing the aged insulation specimens using carbonyl index.

insulation specimens were then attached to a glass slide using an acrylic adhesive to avoid displacement of the specimens during measurement and to avoid contamination of the exposed surfaces as FTIR ATR is a surface sensitive technique (for example, penetration depths are typically on the order of 4 µm at 500 cm^{-1} and 0.5 µm at 4000 cm^{-1} for XLPE and a diamond ATR crystal [34]). A background spectrum was measured in air prior to measurement for spectra subtraction. For each measurement, a total of 64 scans were collected to reduce background noise. Spectra were measured at six locations spanning from the outside to inside edges of the insulation cross-section as shown in Figure 8.

Analysis of the spectra peaks was conducted using OPUS (Bruker) spectroscopy software and a spreadsheet program. The measured backgrounds were first subtracted from the spectra in OPUS and the resulting spectra were exported into a spreadsheet. The spectra were then normalized to the methylene peak at 2920 cm^{-1} (CH_2 asymmetric stretch). Next, two separate baseline corrections were conducted to calculate the carbonyl index:

22
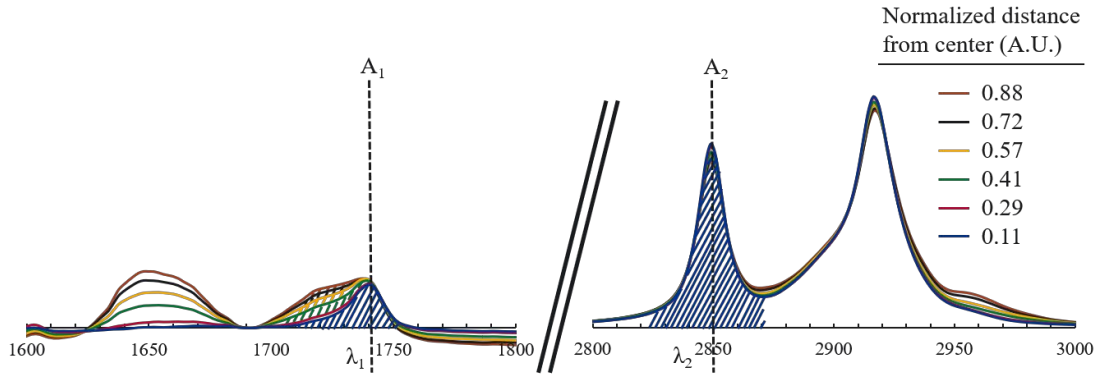
Figure 9. Method for calculation of the carbonyl index.

1. Baseline correction of the spectra to the absorbance at 1680 cm^{-1} (Anaconda EPR), 1740 cm^{-1} (Rockbestos XLPE), and 1690 cm^{-1} (Brand Rex XLPE) based upon the minimum absorbance in the carbonyl region (1690 cm^{-1} to 1750 cm^{-1}). Afterwards, the area under the carbonyl region was integrated ($A_{C=O}$).

2. Baseline correction of the spectra to the minimum absorbance between 2950 cm^{-1} and 3050 cm^{-1}. Afterwards, the area under the methylene region (2750 cm^{-1} to 2870 cm^{-1}) was integrated (A_{C-H}).

An example of the baseline correction methodology is shown in Figure 9. The carbonyl index (CI) was calculated as shown in Equation (4), where A_1 is the absorbance value at wavelength λ_1 and A_2 is the absorbance value at λ_2.

$$CI = \sum_{1750cm^{-1}}^{1690cm^{-1}} \frac{(A_1+A_2)}{2*(\lambda_2-\lambda_1)} \Big/ \sum_{2870cm^{-1}}^{2750cm^{-1}} \frac{(A_1+A_2)}{2*(\lambda_2-\lambda_1)} \qquad (4)$$

4.5   Chemical Composition Measurement Using EDS

The insulation specimens were characterized using energy dispersive X-ray spectroscopy (EDS) to validate total color differences as a metric to evaluate DLO. The specimens were first cut to a thickness between 0.5 to 1.0 mm to enable imaging of their cross-sections. Next, the exposed cross-sections were polished using a combination of liquid nitrogen and a series of increasing grits of sandpaper up to 2500 (approximately 8.5 ± 0.5 μm surface roughness) to smooth the surface. Polished specimens were then washed in a deionized water ultrasonic bath for 30 seconds and dried with a wipe. The polished specimens were mounted onto sample holders using carbon tape prior to scanning electron microscope (SEM) EDS analysis. Images and spectra of the specimen cross-sections were collected using either a JEOL 70001F field emission gun scanning microscope (15 kV accelerating voltage, probe current 13, 20 nm aperture, and 10 mm working distance) or an IT-500 field emission gun scanning microscope (15 kV accelerating voltage, probe current 70, 20 nm aperture, and 10 mm working distance). Two SEMs were used due to experimental constraints. Imaging and EDS were performed in high vacuum mode after coating specimens with 2 nm of iridium as a conductive coating. For the JEOL 70001F, spectra were collected with dual Bruker X-Flash 60 EDS detectors and Esprit software was used for analysis. For the IT-500, spectra were collected using dual Oxford X-max 100 mm detectors and Aztec software was used for analysis.

4.6 Indenter Modulus and Relaxation Constant Measurement

Indenter modulus (IM) values of the aged insulation specimens with intact conductors were measured following IEC/IEEE 62582-2 [35]. Specimens were conditioned following the same procedure as described in Section 4.1 (at least 40 hours at 23°C ± 2°C and 50% ± 10% relative humidity). After conditioning, insulation specimens were placed within a cable clamp assembly of an Indenter Polymer Aging Monitor (IPAM) (IPAM 4M, AMS Corp., Knoxville, Tennessee, USA) as shown in Figure 10a. Insulation specimens were gently clamped within the IPAM to prevent displacement during measurement. An instrumented probe housed within the IPAM indented the external surface of specimens at a loading rate of 5.1 mm/min and a maximum load of 8.9 N, similar to the recommendations of IEC/IEEE 62582-2. Each measurement was conducted under ambient laboratory conditions (approximately 21°C and 30% relative humidity). The indentation process was controlled, and data collected, through the usage of an external pocket PC (see Figure 10b). A total of ten measurements were performed at three locations around the specimen circumference while avoiding indentation from previous measurements within 10 mm of each end of specimens. Per IEC/IEEE 62582-2, indenter modulus (N/mm) was calculated from the slope of the linear portion of the initial force versus deformation curve as shown in Figure 11a and Equation (5), where d_1 and d_2 are the displacements (mm) corresponding to force values of F_1 (1 N) and F_2 (4 N), respectively [35]. In addition to the indenter modulus, the IPAM allows for easy measurement of insulation specimen relaxation constants, τ. After the maximum load (8.9 N) has been reached during indentation, the probe stops moving and relaxation of the polymeric insulation was measured over time (see Figure 11b). The relaxation constant (s) is shown in Equation (6), where F_3 and F_4 are the force (N) values corresponding to measurement times of t_3 (2 s) and t_4 (3 s) after the probe has stopped moving, respectively. The average value and standard deviation of the indenter modulus and relaxation constant are reported after removing the highest and lowest measurement values due to differences in specimen construction, dimensions, and stabilization, according to manufacturer instructions.
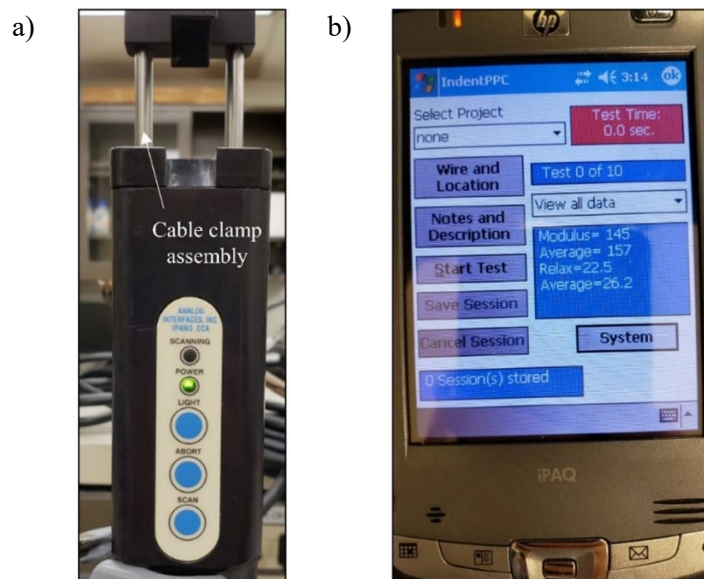
Figure 10. a) Indenter polymer aging monitor (IPAM) and b) pocket PC used for data collection.

$$IM = \frac{F_2 - F_1}{d_2 - d_1} \tag{5}$$

$$\tau = \left| \frac{t_4 - t_3}{\ln \left({F_4}/{F_3} \right)} \right| \tag{6}$$
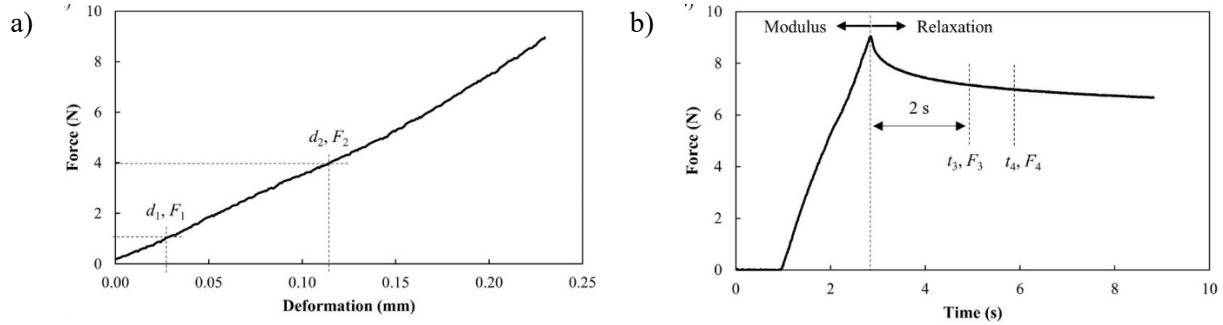
Figure 11. Example plots demonstrating the a) indenter modulus and b) relaxation constant measurement methodology.

5. POLYMER DEGRADATION THEORY

Polymers have become ubiquitous in modern NPP infrastructure. As such, their response to the harsh environments of NPPs has attracted significant interest and been the subject of many studies. There are three primary modes of chemical degradation of polymers in an NPP environment: thermal, radiative, and oxidative. Whenever thermal or radiative degradation occurs in an oxygenated environment these mechanisms become known as thermal-oxidation or photo-oxidation, and oxidative reactions dominate the degradative reaction pathways [36]. For this study, the mechanisms of thermal oxidation are of primary interest.

A polymeric cable insulation specimen may face oxidative atmosphere at above-ambient temperatures in the course of its service lifetime in an NPP [37]. Regarding kinetics, thermal-oxidation is limited to superficial layers of polymeric materials because of the rate-limiting constant of O_2 diffusion into the material [38]. This phenomenon is known as diffusion limited oxidation or DLO. It is important to consider that DLO does not stop oxidation of the material. In fact, prolonged exposure of polymers to thermal-oxidative conditions has been shown to increase the density of the oxidized surface portion of the material which results in shrinkage, tension, and the formation of cracks [39]. Newly formed cracks then facilitate O_2 diffusion deeper into the polymer [39]. Predictably, this behavior is temperature dependent. Practically speaking, however, it is understood that this progression of thermal-oxidative degradation through the thickness of a polymer will eventually render the material defunct.

On a molecular level, thermal oxidation of polymers such as EPR and XLPE primarily occurs through oxidation of aliphatic bonds [40]. This results in the formation of carbonyl, aldehyde, unsaturated vinylene groups, ester, and carboxylic anhydride groups [41]. In addition to the formation of these relatively stable functional groups, radicals can be generated through chain scission of the polymer at elevated temperatures. These radicals can react with other polymer chains in the presence of oxygen to generate hydroperoxide and alkyl radicals and maintain an auto-accelerated oxidative reaction [41]. As a result, the chemical products of thermal oxidation of EPR and XLPE are diverse and difficult to predict with certainty. For the sake of obtaining qualitative information of these materials, then, it is assumed that formation of carbonyl groups is a prominent mechanism of oxidation and is representative of other degradation mechanisms. This can then be evaluated by FTIR using the carbonyl index (CI) which is characterized by the ratio of the

relative intensities absorbed at approximately 1700 cm^{-1} (aldehyde, ester, etc. absorbance) and 2850 cm^{-1} (methylene absorbance). One of the challenges of this approach, however, is the difficulty of mapping degradation through the thickness of a sample using traditional techniques such as FTIR.

Alternate and more accessible methods to analyze oxidation of polymers have recently garnered significant attention in our laboratory to decrease the cost and increase the breadth and detail of DLO studies. One such method which we have developed for this work is the quantitative color analysis of polymer specimens during thermal oxidation. Y. Kemari. et al. first reported the discoloration of XLPE during thermal ageing and demonstrated that the color change was caused by the formation of vinylidene and vinyl groups [42]. More macroscopically, X. Yang et al. showed that thermal-oxidative degradation proceeds in XLPE as a change in color from white transparent to yellow to red at extreme aging conditions and related this to structural changes in the XLPE polymer [43]. As such, it is plausible to assess the ageing condition of polymeric cable insulation through analysis of optical properties. Previous work in our laboratory has demonstrated such a technique as applied to the exterior of thermally oxidized samples [44]. However, the sensitivity of color analysis methods to microscopic phenomena such as DLO has yet to be demonstrated or applied.

Most polymers are thought to undergo oxidative degradation under normal conditions by an autocatalytic process known as auto-oxidation. G. Bolland et al. were first to establish the classically understood mechanism of polymer auto-oxidation which has now become the contemporary theory of auto-oxidation. This process is described in several steps including initiation, chain propagation, chain branching, and termination, as shown in Scheme 1 [45]. Initiation (Scheme 1, (1)) occurs as weak C-H bonds break, leading to the formation of free radicals (R·). These free radicals can then rearrange (Scheme 1 (2)) without terminating the degradation reaction. Regardless, generated radicals quickly react with oxygen to form peroxyl radicals (RO$_2$·) which quickly stabilize into hydro-peroxides (ROOH) through propagation reactions (Scheme 1 (3, 4)). Generated hydro-peroxides can then decompose to form RO· and HO· which results in chain branching reactions (Scheme 1 (5-8)). Ultimately, however, generated radicals form inactive products like carbonyl groups or unsaturated groups through termination reactions (Scheme 1 (9-11)).
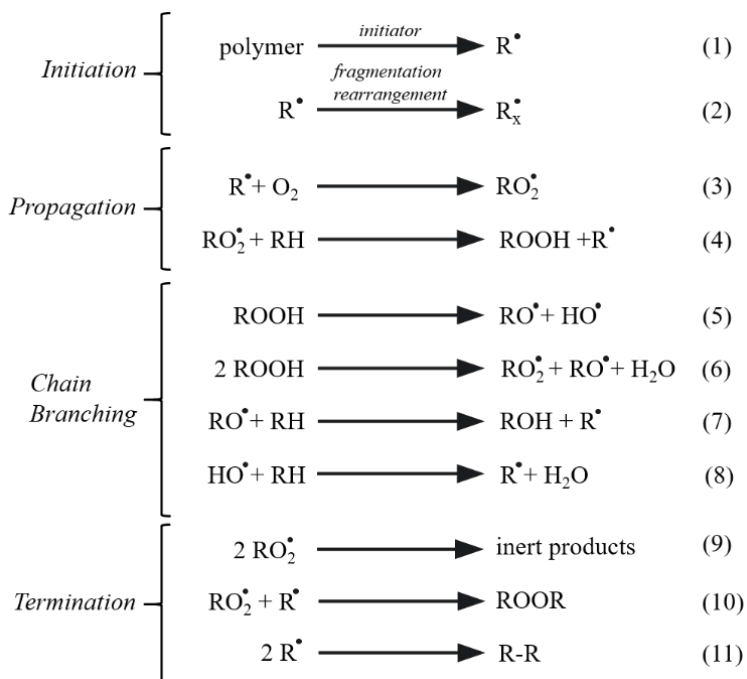
Scheme 1. Basic auto-oxidation scheme [45]

5.1 Model of Diffusion Limited Oxidation

Based upon the above understanding of thermal-oxidative degradation reactions, the non-uniform oxidation of polymers such as EPR or XLPE can be explained by oxygen diffusion theory. When considering thick samples, large thicknesses mean that the rate of oxygen diffusion into the sample becomes heterogenous across the thickness of the sample. Therefore, oxygen consumed by thermal-oxidative reactions cannot be replenished in the interior segments of specimens which leads to regions with reduced oxygen concentration and reduced degradation. For the purposes of modeling DLO behavior, the oxygen consumption rate based upon Scheme 1 [45] is given in Equation (7), where C_1 and C_2 are the overall rate constants associated with the basic auto-oxidation scheme [45] and t is the time.

$$\frac{\partial [O_2]}{\partial t} = -\frac{C_1[O_2]}{1+C_2[O_2]} \tag{7}$$

Following the work of Colin and Verdu [46], Fickian diffusion is incorporated into Equation (7) by balancing the oxygen concentration within the material with the oxygen contribution due to diffusion subtracted from the contribution due to the oxidative reactions. The resulting DLO model is shown in Equation (8), where D is the oxygen diffusivity and ∇ is the del operator [47].

$$\frac{\partial [O_2]}{\partial t} = D\nabla^2[O_2] - \frac{C_1[O_2]}{1+C_2[O_2]} \tag{8}$$

To simplify analysis of Equation (8), normalization parameters are commonly introduced [48]. Assuming constant diffusivity, the continuity equation (non-dimensionalized) is given in Equation (9), where τ is the non-dimensionalized time ($\tau = tD/L^2$ and L is the reference thickness) and θ is the relative oxygen concentration ($[O_2]/[O_2(0)]$ and $[O_2(0)]$ is the oxygen concentration at the external surface). In addition, the non-dimensionalized DLO model parameters are given in Equation (10) and Equation (11) for β and α, respectively, where φ is the oxidation rate, φ_0 is the oxidation rate at ambient equilibrium (non-DLO conditions), ρ is the material density, P_{ox} is the oxygen permeability of the material, and p_0 is the ambient oxygen partial pressure [48].

$$\frac{\partial \theta}{\partial \tau} = \nabla^2 \theta - \frac{\alpha \theta}{1+\beta\theta} \tag{9}$$

$$\beta = \frac{\varphi_0 - \varphi/\theta}{\varphi - \varphi_0} \tag{10}$$

$$\alpha = (\beta + 1)\frac{\varphi_0 L^2 \rho}{P_{ox} p_0} \tag{11}$$

Thus, the resulting DLO model is only dependent upon the experimentally measured values for oxygen permeability and oxygen consumption at the test and non-DLO conditions. It is important to note that the DLO model of Equation (9) is asymptotic at $\theta = 1$; thus, the initial condition at $\tau = 0$ is typically given as $\theta(\tau = 0) = 0.99$. In addition, it is also important to note that the oxygen permeability of Equation (11) does not vary with time or location, which may overestimate oxidation within the material [49].

While the functional form of Equation (9) is similar to the commonly encountered heat equation, the addition of a nonlinear forcing function makes solving for an analytical expression difficult. Therefore, the DLO model is solved in this study via COMSOL Multiphysics® (www.comsol.com) using the coefficient form partial differential equation module.

6. CHARACTERIZATION RESULTS

The concern has been raised that DLO may lead to significant overestimation of the operational lifetime of electrical cable components qualified using highly elevated accelerated aging conditions [19,20]. Uncertainties still exist regarding the impact of DLO on NPP electrical cable qualification, such as the threshold temperatures and exposure durations beyond which DLO is prevalent and how exceeding these thresholds could affect conclusions drawn during historical cable qualification. In this report, two common nuclear cable insulation materials [3]—ethylene-propylene-rubber and cross-linked polyethylene—were aged at four temperatures (121°C, 136°C, 150°C, and 165°C) and varying exposures to determine the threshold conditions at which DLO occurs. A variety of characterization techniques were employed to assess DLO and to supply more complete information to regulators, operators, and other decision-makers about the long-term operation of nuclear electrical cables exposed to DLO effects. All measurements were compared to the as-received specimens to avoid issues with aging history.

6.1 Mechanical Characterization

A common failure threshold of 50% EAB retention (rEAB) was used for all insulation specimens. Insulation specimen Anaconda EPR exhibited immediate and significant decreases in measured EAB values at all analyzed accelerated aging temperatures (Figure 12a). Significantly, Anaconda EPR reached its failure threshold at all analyzed temperatures within the time limitations of this study. In contrast, ultimate tensile strength (UTS) values did not decrease in tandem with EAB for Anaconda EPR. Rather, the degradation of UTS was delayed when compared to EAB. Finally, the UTS of Anaconda EPR did degrade with increasing duration of accelerated aging and did trend well with EAB. Insulation specimen Rockbestos XLPE exhibited degradation of EAB to the failure threshold at temperatures above 150 °C. The EAB values also decreased at lower temperatures but not as readily as Anaconda EPR and did not reach the failure threshold within the confines of this study. The UTS behavior of Rockbestos XLPE was similar to that of Anaconda EPR in that it trended well with EAB but exhibited a delayed response. No analyzed timepoint of Rockbestos XLPE exhibited UTS degradation below 80% of the initial UTS. Insulation specimen Brand Rex XLPE was the most stable specimen to accelerated aging as evidenced by its retention of EAB and UTS compared to Anaconda EPR and Rockbestos XLPE. Brand Rex XLPE achieved the failure threshold of 50% EAB retention only when aged at 165 °C. Some decline in EAB was observed at 150 °C and the material was insensitive to aging at 136 °C and 121 °C according to EAB measurements. As expected from the other material types, the UTS of XPLE 2 was more insensitive to aging than EAB and did not display meaningful property loss except at prolonged exposure at 165 °C. Aging duration required to reach the failure threshold of each insulation specimen at the temperatures tested are listed in Table 7 and Table 8. A sigmoidal function (Equation 12) was used to predict time to threshold for specimens that did not reach 50% rEAB within the confines of this study where a, b, and c are parameters for sigmoidal shape and t is the exposure time in days (Figure A1).

$$EAB = \frac{a}{1+e^{-b(log_{10}t-c)}}$$ (12)

Table 7. Experimental and sigmoidal function predicted (where experiment time-out) aging duration to reach 50% EAB retention (rEAB) threshold of specimens Anaconda EPR, Rockbestos XLPE, and Brand Rex XLPE at analyzed accelerated aging temperatures.

Specimen ID	Time to 50% rEAB at 121 °C (days)	Time to 50% rEAB at 136 °C (days)	Time to 50% rEAB at 150 °C (days)	Time to 50% rEAB at 165 °C (days)
Anaconda EPR	210	80	21	7
Rockbestos XLPE	400	120	56	13
Brand Rex XLPE	420	425	70	18

Table 8. Experimental and predicted aging duration to reach 50% EAB (absolute) threshold of specimens Anaconda EPR, Rockbestos XLPE, and Brand Rex XLPE at analyzed accelerated aging temperatures.

Specimen ID	Time to 50% EAB at 121 °C (days)	Time to 50% EAB at 136 °C (days)	Time to 50% EAB at 150 °C (days)	Time to 50% EAB at 165 °C (days)
Anaconda EPR	380	120	33	11
Rockbestos XLPE	500	150	62	16
Brand Rex XLPE	580	1100	110	24
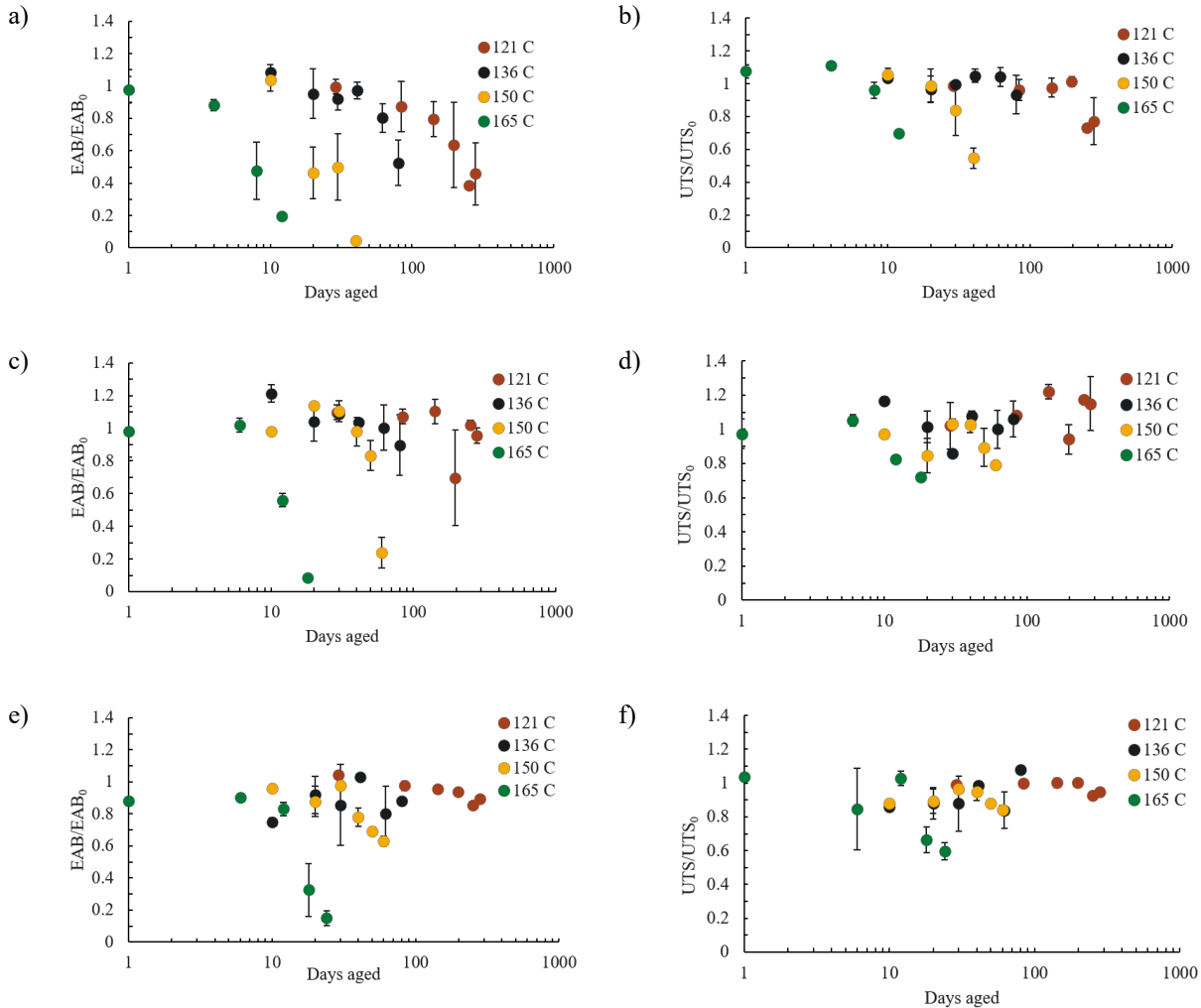
Figure 12. Obtained results from EAB and ultimate tensile strength analyses of cable specimens. a) Anaconda EPR EAB results after accelerated aging at select temperatures b) Anaconda EPR UTS results after accelerated aging at select temperatures c) Rockbestos XLPE EAB results after accelerated aging at select temperatures d) Rockbestos XLPE UTS results after accelerated aging at select temperatures e) Brand Rex XLPE EAB results after accelerated aging at select temperatures and f) XLPE UTS results after accelerated aging at select temperatures.

Accelerated aging was performed beyond the durations indicated in Figure 12 however data points far beyond the failure threshold were removed for clarity. EAB and UTS results including these results are found in Figure A2.

6.2   Total Color Difference

Total color difference (ΔE^*_{ab}) analyses of specimen cross-sections were performed. A 10 % ΔE^*_{ab} difference threshold from sample center (n = 0.5) to the exterior sample edge (n = 0.95) was used to determine whether DLO was significant for the analyzed specimen at a given temperature [19]. The interior edge (n = 0.05) was ignored for the purposes of this study due to irregularities of the shape of the inner diameter surface and complications in surface aging hypothesized to be associated with conductor materials. Analyses were performed on the three insulation specimens selected with results ranging from DLO being significant at all temperatures (Rockbestos XLPE) to DLO being insignificant at all temperatures (Brand Rex XLPE).

Total color difference line and surface profiles of Anaconda EPR are shown in Figure 13. DLO threshold calculation results for specimen Anaconda EPR are reported in Table 9. Individual specimen calculations used to generate Table 9 are reported in Table A1. Specimen Anaconda EPR did not display significant DLO at the exterior edge when aged at 121 °C (Figure 13a). Some heterogenous oxidation was observed on the internal edge. A select surface ΔE^*_{ab} profile is depicted in Figure 13b to help visualize a cable insulation specimen without significant DLO. Figure 13c displays ΔE^*_{ab} of Anaconda EPR aged at 136 °C. DLO was observed to be significant for specimen Anaconda EPR at this temperature by the magnitude of the change of ΔE^*_{ab} from the center to the external edge (Table 9). Heterogenous aging was also observed on the internal edge in Figure 13c but is ignored in the analysis as detailed above. A select surface profile of Anaconda EPR aged at 136 °C is also shown in Figure 13d. It was observed that ΔE^*_{ab} significantly increased near the location where the conductor had been, as well as on the exterior edge of the cable insulation specimen. Figure 13e displays ΔE^*_{ab} of Anaconda EPR aged at 150 °C for various durations. Here, it was observed that internal heterogenous aging began to dominate the oxidation of Anaconda EPR cable insulation specimens at aging temperatures of 150 °C. In fact, the increase in ΔE^*_{ab} at the internal edge for Anaconda EPR samples aged at 150 °C extended out to n = 0.5 at the point where the sample was failing according to EAB analyses. Regardless, external DLO was found to be significant for Anaconda EPR aged at 150 °C (Table 9). A select surface profile of Anaconda EPR aged at 150 °C is shown in Figure 13f. The significant increases in internal DLO were observed as areas of high ΔE^*_{ab} (shown in red) near the internal edges of the sample. The misshapen structure of the specimen shown in Figure 13f was a result of compression by the clamp during accelerated aging. Figure 13g and h displays ΔE^*_{ab} of Anaconda EPR aged at 165 °C. It was observed that internal heterogenous aging was not as significant in Anaconda EPR samples aged at 165 °C as compared to 150 °C. External DLO was found to be significant for Anaconda EPR aged at 165 °C (Table 9). Significant progression of internal heterogenous aging was observed as high ΔE^*_{ab} extending out from the interior edge to the sample center. Neither Figure 13g nor Figure 13e display data from samples that had significantly surpassed their failure thresholds as determined by EAB (50 and 60 days of aging at 150 °C and 16- and 20-days aging at 165 °C).

Table 9. Average ΔE^*_{ab} % increase from sample center to sample edge values of specimen Anaconda EPR shown for each accelerated aging temperature.

Aging Temperature (°C)	Average ΔE^*_{ab} increase from sample center to sample edge (%)	Meets DLO threshold?[‡]
121	7.3 ± 4.6	No
136	12.8 ± 3.8	Yes
150	14.3 ± 5.8	Yes
165	15.0 ± 10.8	Yes

[‡]DLO threshold is at least 10% ΔE^*_{ab} difference
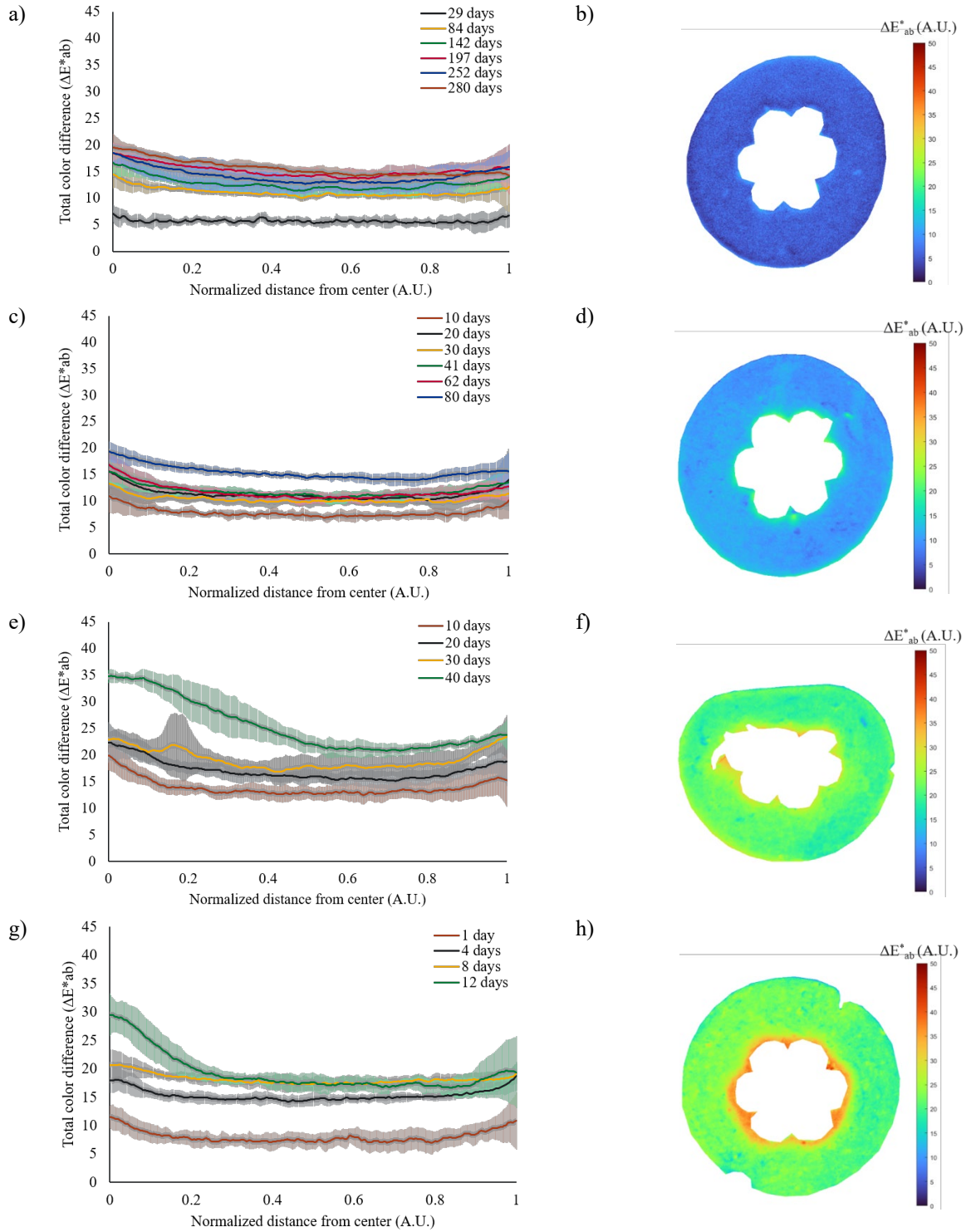
Figure 13. Total color difference (ΔE^*_{ab}) plots and surface images of specimens. a) compiled ΔE^*_{ab} plots for Anaconda EPR specimens aged at 121 °C b) ΔE^*_{ab} surface plot of Anaconda EPR aged at 121 °C for 29 days c) compiled ΔE^*_{ab} plots for Anaconda EPR specimens aged at 136 °C d) ΔE^*_{ab} surface plot of Anaconda EPR aged at 136 °C for 20 days e) compiled ΔE^*_{ab} plots for Anaconda EPR specimens aged at 150 °C f) ΔE^*_{ab} surface plot of Anaconda EPR aged at 150 °C for 20 days g) compiled ΔE^*_{ab} plots for Anaconda EPR specimens aged at 165 °C h) ΔE^*_{ab} surface plot of Anaconda EPR aged at 165 °C for 12 days.
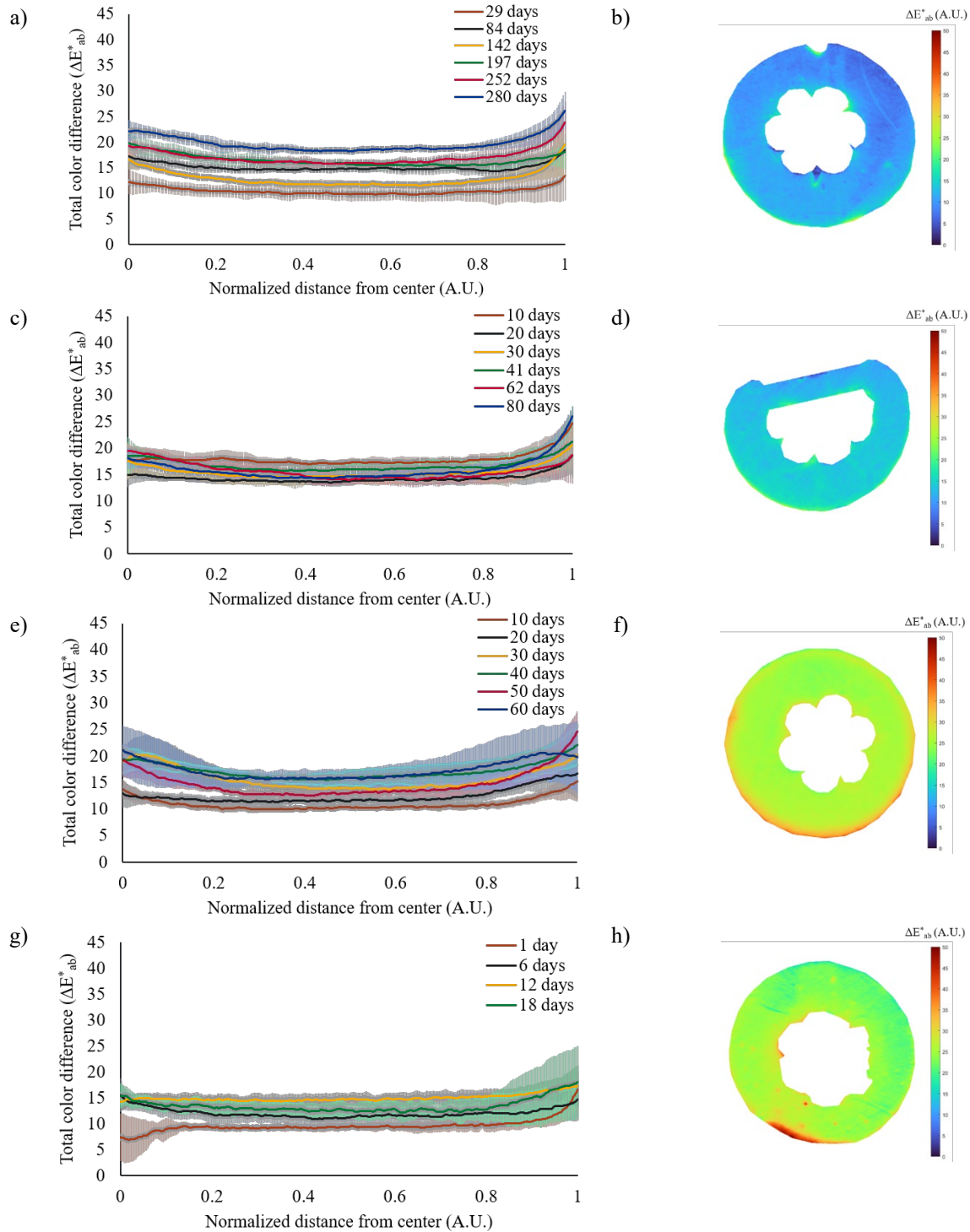
Figure 14. Total color difference (ΔE^*_{ab}) plots and surface images of specimens a) compiled ΔE^*_{ab} plots for Rockbestos XLPE specimens aged at 121 °C b) ΔE^*_{ab} surface plot of Rockbestos XLPE aged at 121 °C for 29 days c) compiled ΔE^*_{ab} plots for Rockbestos XLPE specimens aged at 136 °C d) ΔE^*_{ab} surface plot of Rockbestos XLPE aged at 136 °C for 20 days e) compiled ΔE^*_{ab} plots for Rockbestos XLPE specimens aged at 150 °C f) ΔE^*_{ab} surface plot of Rockbestos XLPE aged at 150 °C for 20 days g) compiled ΔE^*_{ab} plots for Rockbestos XLPE specimens aged at 165 °C h) ΔE^*_{ab} surface plot of Rockbestos XLPE aged at 165 °C for 18 days.

Table 10. Average ΔE^*_{ab} % increase from sample center to sample edge values of specimen Rockbestos XLPE shown for each accelerated aging temperature.

Aging Temperature (°C)	Average ΔE^*_{ab} increase from sample center to sample edge (%)	Meets DLO threshold?[‡]
121	17.0 ± 7.9	Yes
136	20.5 ± 6.6	Yes
150	33.2 ± 7.9	Yes
165	21.8 ± 7.1	Yes

[‡]DLO threshold is at least 10% ΔE^*_{ab} difference

Total color difference plots of Rockbestos XLPE are shown in Figure 14. Total color difference results of Rockbestos XLPE aged at 121 °C are reported in Figure 14a, specimens aged at 136 °C are reported in Figure 14c, specimens aged at 150 °C are reported in Figure 14e, and Rockbestos XLPE specimens aged at 165 °C are reported in Figure 14g. Select surface profiles of Rockbestos XLPE aged at 121 °C, 136 °C, 150 °C, 165 °C are presented in Figure 14b, d, f, and h, respectively. DLO threshold calculation results for specimen Rockbestos XLPE are reported in Table 10. Individual specimen calculations used to generate Table 10 are reported in Table A2. Surface profiles of Rockbestos XLPE are shown in Figure 14. An increase in ΔE^*_{ab} at specimen centers (n = 0.5) associated with increasing exposure durations was observed with all samples. Specimen Rockbestos XLPE did display significant external DLO when aged at all tested temperatures (Figure 14a-d). It was also observed in Figure 14a-d that internal DLO was not as significant a factor as it had been in sample Anaconda EPR. Figure 14g does not display data from samples that had significantly surpassed their failure thresholds as determined by EAB (24- and 30-days aging at 165 °C).

ΔE^*_{ab} plots of Brand Rex XLPE are shown in Figure A3 for brevity. Total color difference results of Brand Rex XLPE aged at 121 °C are reported in Figure A3a, specimens aged at 136 °C are reported in Figure A3c, specimens aged at 150 °C are reported in Figure A3e, and Rockbestos XLPE specimens aged at 165 °C are reported in Figure A3g. DLO threshold calculation results for specimen Brand Rex XLPE are reported in Table 11. Individual specimen calculations used to generate Table 11 are reported in Table A3. Select surface profiles of Brand Rex XLPE aged at 121 °C, 136 °C, 150 °C, 165 °C are presented in Figure A3b, d, f, and h, respectively. An increase in ΔE^*_{ab} at specimen centers (n = 0.5) associated with increasing exposure durations was observed with all samples. Specimen Brand Rex XLPE did not display significant external DLO at any tested temperatures (Table 11). Reported data for Brand Rex XLPE does not display values from samples that had significantly surpassed their failure thresholds as determined by EAB (30 days aging at 165 °C).

Table 11. Average ΔE^*_{ab} % increase from sample center to sample edge values of specimen Brand Rex XLPE shown for each accelerated aging temperature.

Aging Temperature (°C)	Average ΔE^*_{ab} increase from sample center to sample edge (%)	Meets DLO threshold?[‡]
121	2.7 ± 1.9	No
136	5.0 ± 3.5	No
150	6.4 ± 2.7	No
165	6.0 ± 5.0	No

[‡]DLO threshold is at least 10% ΔE^*_{ab} difference

Figure 15. Nanoindentation results from specimen Anaconda EPR aged at select temperatures and durations a) change in hardness (HRA) of Anaconda EPR reported as a function of distance from the center of the specimen and b) change in elastic modulus (λ) of Anaconda EPR reported as a function of distance from the center of the specimen.

ΔE^{*}_{ab} comparisons of Anaconda EPR and Rockbestos XLPE samples aged for similar durations at different accelerated aging temperatures are reported in Figure 16. The corresponding ΔE^{*}_{ab} comparison for specimen XLPE is included in the appendix Figure A4 for brevity. Figure 16a displays the increase in overall ΔE^{*}_{ab} of specimen Anaconda EPR at higher aging temperatures, with the largest stepwise difference observed to occur between aging temperatures 150 °C and 165 °C. Similarly, the increase in overall ΔE^{*}_{ab} for specimen XLPE is shown in Figure 16b where step-wise increases in ΔE^{*}_{ab} at the center of the sample remained relatively small but significant differences between aging temperatures were observed at the sample internal and external edges. The most significant differences were once again observed to occur between aging temperatures of 150 °C and 165 °C. Figure A4 demonstrates the insensitivity of Brand Rex XLPE to heterogenous aging at all accelerated aging temperatures tested. Although heterogenous aging was not observed there was a significant increase in ΔE^{*}_{ab} at the sample center (n = 0.5) with increasing aging duration reported.

6.3   Additional Characterization Methods

Results from nanoindentation analysis of specimen Anaconda EPR are reported in Figure 15. Select samples were chosen for nanoindentation analysis to validate the color analysis method reported above. It was observed that the change in hardness of Anaconda EPR was more significant at 165 °C accelerated aging conditions than at 121 °C. Furthermore, it was observed that more significant changes in hardness occurred on the interior edge of specimen Anaconda EPR aged at 165 °C for 16 days, whereas the other measured samples did not display significant deviations in hardness from the sample center (n = 0.5). This
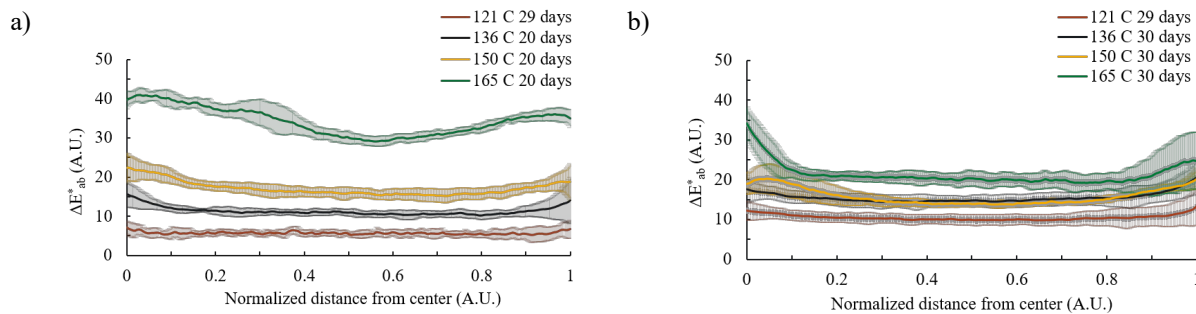
Figure 16. a) compiled ΔE^{*}_{ab} plots for Anaconda EPR specimens aged at various temperatures but constant durations b) compiled ΔE^{*}_{ab} plots for Rockbestos XLPE specimens aged at various temperatures but constant durations
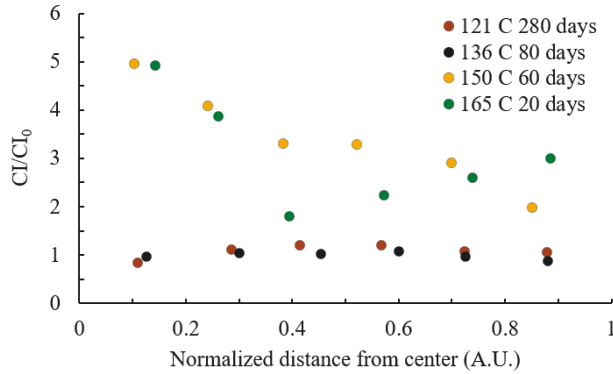
Figure 17. Normalized carbonyl index (CI) of specimen Anaconda EPR aged at various temperatures and for select durations used for verification of color analysis.

trend was also observed when observing changes in elastic modulus with increasing accelerated aging temperature and exposure.

Carbonyl Index (CI) measurements of specimen Anaconda EPR are reported in Figure 17. Select samples were chosen from maximum exposure durations for each accelerated aging temperature to validate the color analysis method. It was observed that CI of specimen Anaconda EPR did not vary significantly between aging at 121 °C and 136 °C and the magnitude of CI was not observed to change significantly over the radius of the specimens. However, on increasing aging temperature to 150 °C a significant increase in overall CI was observed. Furthermore, the magnitude of CI was observed to decrease from the interior edge of the sample to the exterior edge of the specimen. When CI was measured for specimen Anaconda EPR aged at 165 °C it was observed that CI decreased from the interior edge to the center of the specimen and then increased from the specimen center to the outside edge. Further CI analyses of specimens Rockbestos XLPE and Brand Rex XLPE are reported in Figure A5.

Results from cable indenter measurements of specimen Anaconda EPR are reported in Figure 18. Select samples were chosen for cable indenter analysis to investigate the effect of DLO. It was found that IM of insulation specimens did not increase significantly at temperatures where DLO was observed (Figure 18a). However, a subtle increase in IM was observed at 121 °C where DLO was not observed to occur during DLO threshold determinations. Similarly, no significant trend in τ was observed in samples where DLO was observed (Figure 18b). However, a significant decrease in τ was observed at extended aging durations at 121 °C where DLO was not observed to occur.

Results from EDS analysis of specimen Anaconda EPR are reported in Figure 19. Select samples were chosen for EDS analysis to validate the color analysis method reported above. Additional verification samples are reported in Figure A6. It was observed that Anaconda EPR did not display significant heterogenous aging after aging at 121 °C for the selected duration (Figure 19a). When aging temperature was increased to 165 °C some heterogenous aging was observed at the external edge (n = 0.95) at low aging duration, with more significant heterogeneities observed at prolonged aging duration. A select image of specimen Anaconda EPR acquired using backscatter mode is presented in Figure 19b. Many lighter areas were observed in the specimen. Lighter areas observed using backscatter techniques correspond to areas with higher inorganic content. For these specimens' inorganic content was assumed to comprise antioxidants and other fillers, but precise material compositions were not available.
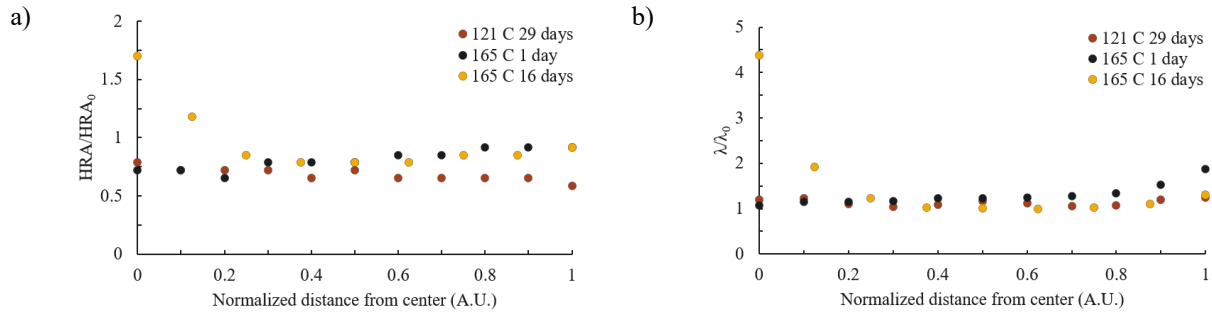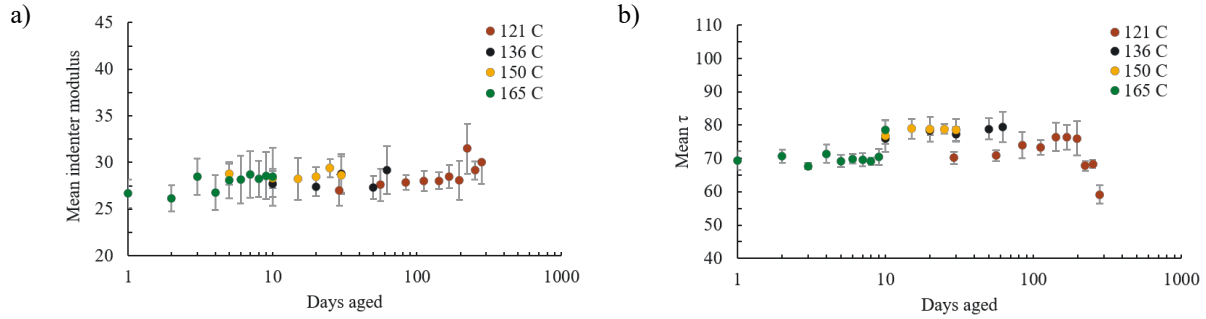
Figure 18. Cable indenter results from specimen Anaconda EPR aged at select temperatures and durations a) mean IM of Anaconda EPR after aging and b) mean τ of Anaconda EPR after aging.

7. DISCUSSION

Heterogenous oxidation of materials during accelerated aging experiments is a common phenomenon, as every material has a unique chemical response to oxidation and a unique oxygen permeability of the material structure. When considering polymers used in NPP low voltage electrical cables, researchers must also consider the effect of inorganic additives, antioxidants, conductors, and processing defects on the response of a cable to accelerated aging. Significant research effort has been dedicated globally to fundamentally understand DLO [37,50–54]. Notably, significant insights into the subject have been forthcoming from Sandia National Laboratory, K. Gillen, and M. Celina [37,55–58]. Although the fundamental understanding of DLO has advanced significantly and the techniques to investigate DLO have become more advanced, the question remains: how significant has DLO been in historical qualifications and how have accelerated aging processes affected long term cable performance confidence.

A drawback in DLO research and a significant hindrance toward understanding this phenomenon is the large sample sets with complex and time-consuming analyses required to make broader claims. To better be able to address the gaps in literature we developed a fast and quantitative color analysis technique which we used to identify DLO thresholds for cable insulation specimens. Therefore, this work has three goals: first, to investigate whether DLO significantly affects lifetime prediction from cable qualification studies. Second, to identify the thresholds at which DLO occurs in three widely used NPP low voltage electrical
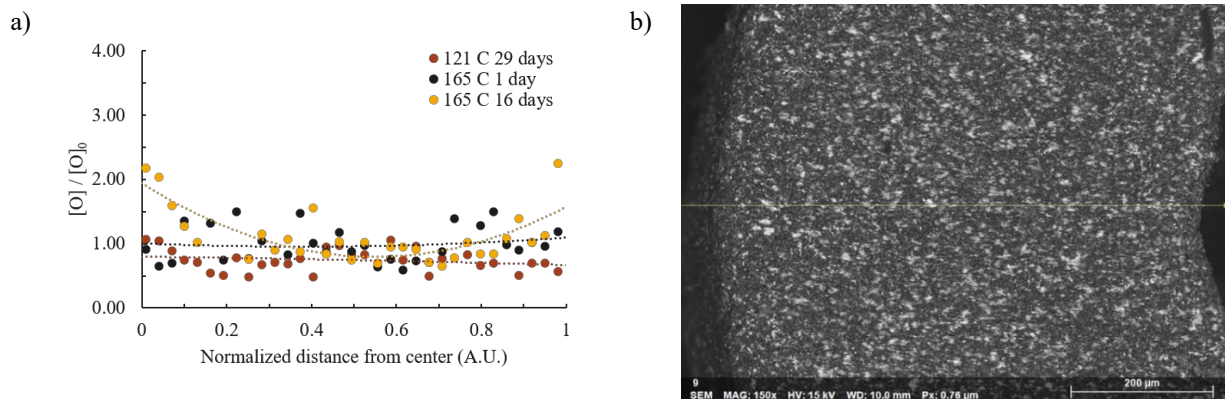

Figure 19. EDS results from Anaconda EPR aged at select temperatures and durations a) EDS analyses where [O] is defined as oxygen concentration and b) an SEM image collected using backscatter techniques of an Anaconda EPR specimen which demonstrates the high inorganic content assumed to be antioxidants and other additives.

cable insulation specimens, which were harvested from active service. Finally, to validate and demonstrate the developed color analysis technique for the identification of DLO in polymeric cable insulation materials.

7.1 Verification of Total Color Difference as Metric to Measure DLO

Prior to usage of the total color difference method as a tool to determine DLO thresholds it was vital to verify the method by traditional DLO analysis techniques to support its use for this application. Therefore, the accuracy and precision of the total color difference method were discussed first and compared to oxygen content as measured by EDS, carbonyl index as measured by FT-IR microscopy, and elastic modulus as obtained by nanoindentation. Finally, the total color difference method was compared to an idealized model of DLO.

Verification of the total color difference method was carried out on select Anaconda EPR samples using the methods previously discussed. Verification samples were selected based on the expected presence of heterogenous oxidation. Data obtained from these methods was normalized and plotted on common axes to facilitate method evaluation (Figure 20). Aging temperatures and durations were selected to represent two specific scenarios: 1) a specimen with no observable DLO and 2) two specimens with increasing magnitude of DLO with increasing aging duration. It was therefore expected that in the first condition selected the total color difference method would not return a false positive. On the other hand, for the method to have validity it is important that it can detect increasing heterogeneity as aging continues. Total color difference is first compared to the other presented methods and then compared with a theoretical model.

Measuring oxygen concentration is a direct method of tracking oxidation effects on a material. Several methods exist for measuring oxygen content, two of the most prevalent in literature being EDS and X-ray photoelectron spectroscopy. Of these two, EDS is more suited for evaluation of large sample sets and as such was selected for comparison. It was observed in Figure 20a and b that the overall oxygen content did not exhibit heterogenous behavior, as would be expected for a sample undergoing DLO. It is worth mentioning that the error between points is significant in EDS and particularly so in these systems where inorganic additive aggregates are responsible for oxygen content in the sample above that due to polymer thermo-oxidation. As was mentioned before, the exact chemical compositions of the obtained cable insulation specimens are not available. It was concluded that additives such as TiO_2 were certainly present in specimen Anaconda EPR. This conclusion was reached after EDS measurements showed significant spikes in Ti and O concentration when analyzing portions of the specimen with high inorganic concentrations as shown by the backscatter imaging mode (Figure 19b). Apart from this contribution, a significantly increasing trend in O concentration was observed in Figure 20c with polymer aging. These results were in good agreement with ΔE^*_{ab} results. However, data collected by total color difference analysis did contrast with EDS data in Figure 20b. In Figure 20b EDS results suggest no heterogenous oxidation was observed on either edge of the specimen. However, ΔE^*_{ab} results suggested that DLO did in fact occur in these conditions. Therefore, although EDS data supported the validity of ΔE^*_{ab} analyses, additional work is needed to understand differences observed.

Nano-indentation is another common technique in DLO literature used to measure microscopic mechanical property differences across the width of a sample. Although nano-indentation is commonly known to produce consistent and accurate data, sample preparation and the analysis technique itself are known to be non-conducive to high-throughput studies. It was observed in Figure 20a that reduced elastic modulus results did not exhibit heterogenous behavior on either end of the Anaconda EPR specimen. This was found to be in good agreement with collected ΔE^*_{ab} data. Furthermore, whereas EDS analysis suggested no heterogenous behavior in Figure 20b, nanoindentation results demonstrated that DLO was present on the external edge of the specimen, in good agreement with collected ΔE^*_{ab} results. Finally, it was observed in Figure 20c that nanoindentation and ΔE^*_{ab} were in good agreement regarding the heterogenous aging of the specimen. Therefore, further confidence in the ΔE^*_{ab} method was generated *via* confirmation using
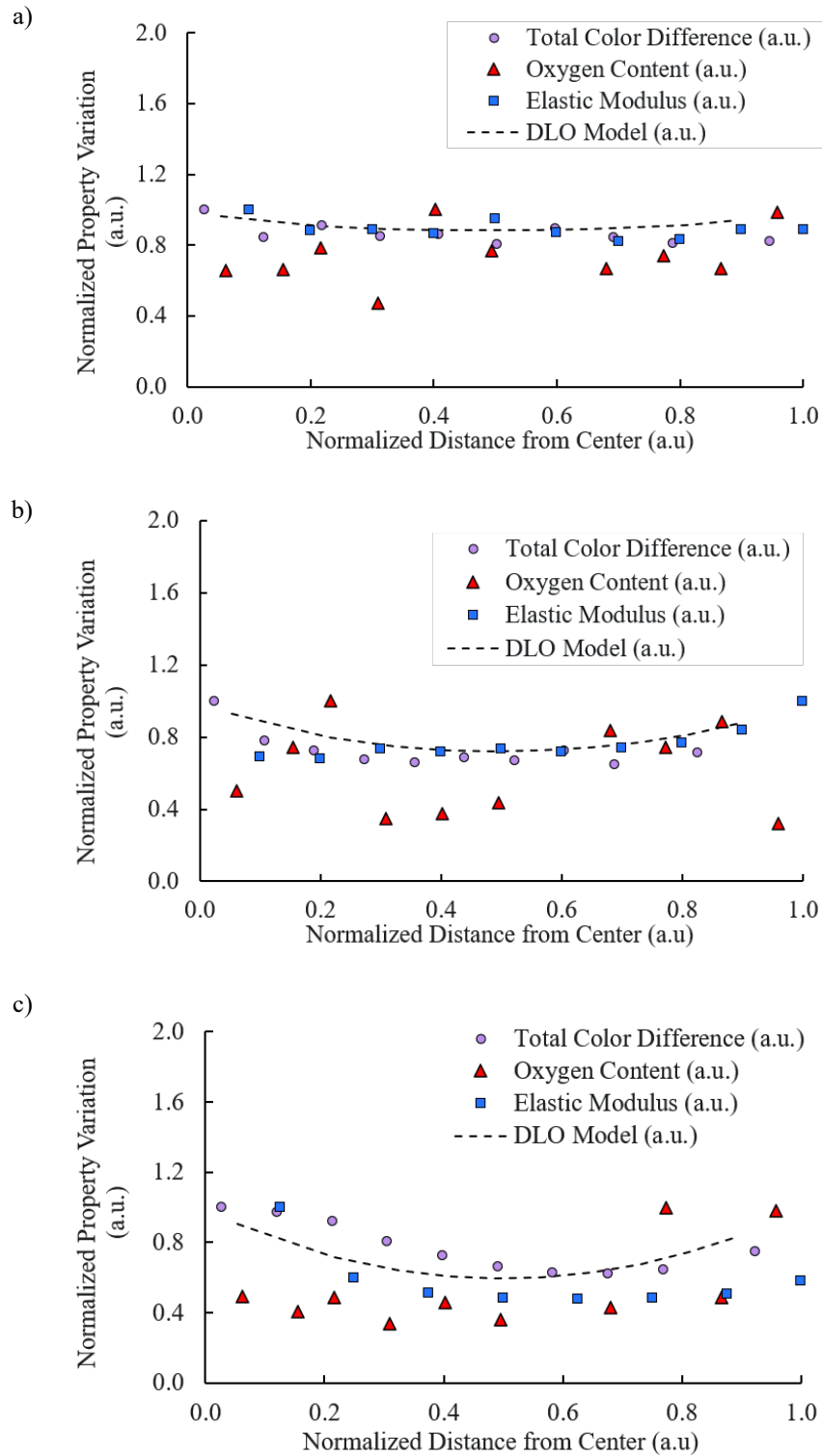
Figure 20. Normalized results of select Anaconda EPR specimens used for verification of the total color difference analysis method a) results from an Anaconda EPR specimen aged at 121 °C for 29 days b) results from an Anaconda EPR specimen aged at 165 °C for 1 day and c) results from an Anaconda EPR specimen aged at 165 °C for 16 days.

nanoindentation. Especially important was the resolution of the inconclusive EDS data in Figure 20b. A third and final verification method (FT-IR microscopy) was then employed to repeat the observation of DLO in Figure 20b as well as to evaluate other selected conditions.

Carbonyl index (CI) is a direct method of measuring oxidation reactions occurring within a material. Although typical FTIR instruments do not have the capability to map a surface as is necessary when studying heterogenous oxidation, specialized FTIR microscopes are designed to obtain spectra across the surface of a sample. Using such an instrument it becomes possible to investigate heterogenous oxidation in polymeric materials, although detailed analyses are hampered by the slow rate of data acquisition. It was observed in Figure 21 that CI trends were in good agreement with ΔE^*_{ab} results. This was particularly noticeable when observing Anaconda EPR specimens aged at 150 and 165 °C. Further verification results are reported in Figure A7. Importantly, the obtained FTIR data confirmed the accuracy of the $\Delta E*ab$ analysis and related color change to oxidation reactions occurring within the polymer.

The DLO model used herein was generated to compare obtained results with idealized DLO (model parameters of α = 5.0 and 8.0 at 121 °C and 165 °C, respectively and β = 1). It was observed in Figure 20 that ΔE^*_{ab} and nanoindentation followed the generated model especially well. This lent further confidence in the ΔE^*_{ab} method. Interestingly, comparing the model to real data in Figure 20c shows that specimen Anaconda EPR underwent accelerated heterogenous aging on the interior edge of the sample. This is potentially attributable to catalysis of oxidation reactions by copper impurities remaining from the conductor removal process.[59] Based on these results it was concluded that ΔE^*_{ab} is a suitable method to evaluate heterogenous aging in polymers. Furthermore, some advantages of this technique were apparent during the present work. Firstly, rapid sample preparation and high throughput facilitated investigating a large sample set. Also of significant importance was the quality of the data, which was found to have similar sensitivity to EDS and nano-indentation.
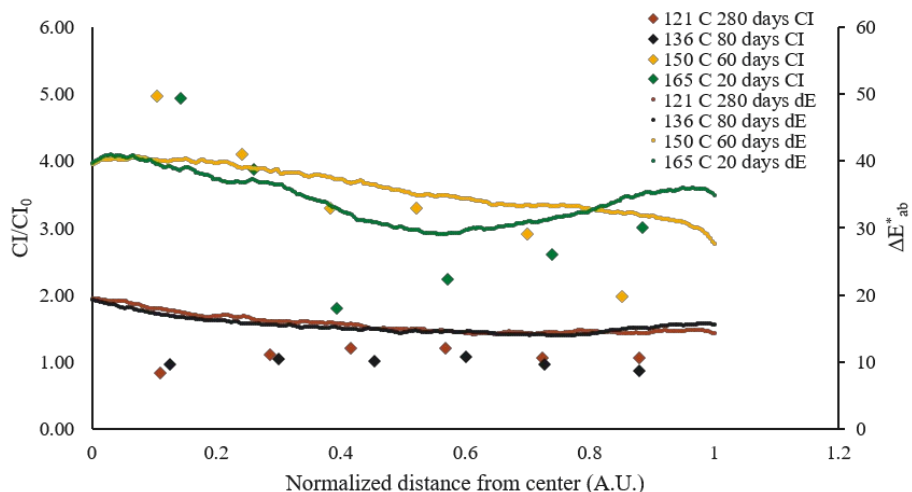
Figure 21. Normalized carbonyl index (CI) of specimen Anaconda EPR aged at various temperatures and for select durations overlaid with commensurate ΔE^*_{ab} results.
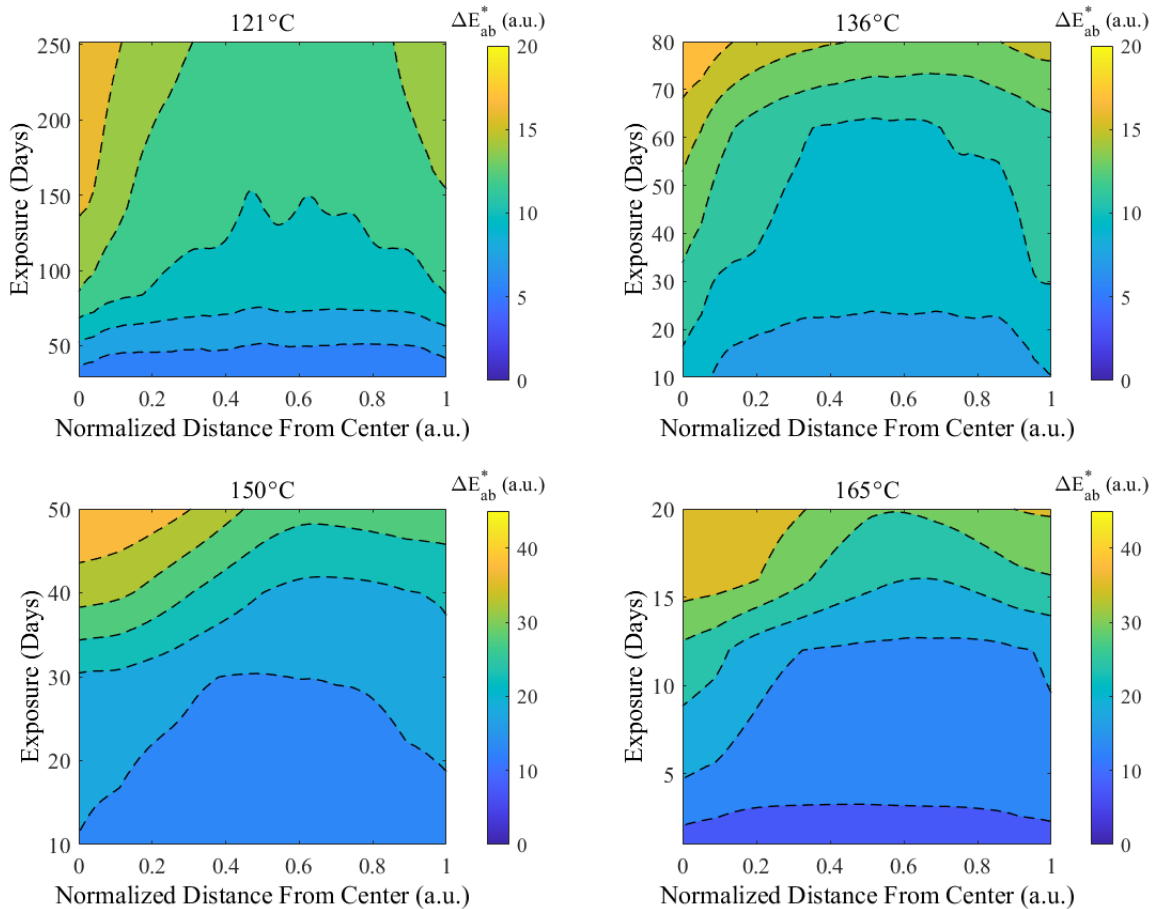
Figure 22. Three-dimensional plots of ΔE^*_{ab} as a function of exposure time (days) and normalized distance from center for specimen Anaconda EPR.

7.2   DLO Onset Based on Exposure Time

Onset behavior of DLO is significant when considering accelerated aging experiments. One remaining knowledge gap concerns DLO onset behavior based on exposure time. Previous work has reported that the magnitude of DLO increases with exposure duration [49]. Three-dimensional plots of ΔE^*_{ab} as a function of exposure time and distance from center were generated for each investigated specimen to further visualize this phenomenon. Figure 22 depicts these graphs for specimen Anaconda EPR. Figure 23 depicts these same for Rockbestos XLPE, and plots Brand Rex XLPE are reported in Figure 24. As has been mentioned previously, DLO as a phenomenon affects each material uniquely. Therefore, it was not unexpected to observe more than a single trend in the present work. It was observed in Figure 22 that the magnitude of the observed DLO effect increased with increasing exposure time in specimen Anaconda EPR. This effect was especially visible at 136 °C and 165 °C. In contrast, specimens Rockbestos XLPE and Brand Rex XLPE were not observed to exhibit this response. Specimen Rockbestos XLPE aged heterogeneously (Figure 23) however DLO remained confined to the extreme edges of the sample. Specimen Brand Rex XLPE was observed to age homogenously at all temperatures (Figure 24). Interestingly, none of the specimens exhibited what might be considered standard DLO behavior (Figure 21).
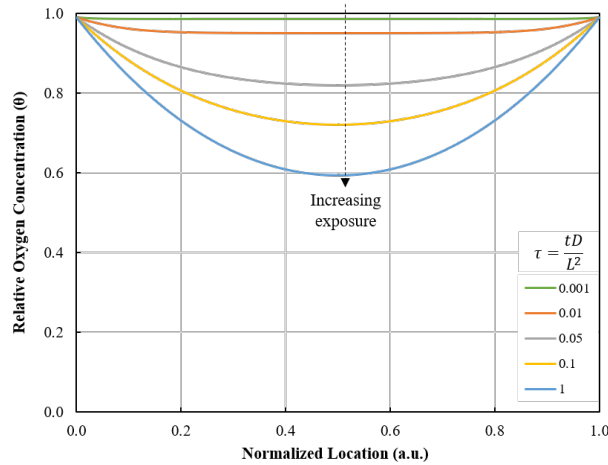
Figure 21. Idealized model of DLO progression with increasing exposure time ($\alpha = 8.0$ and $\beta = 1.0$).
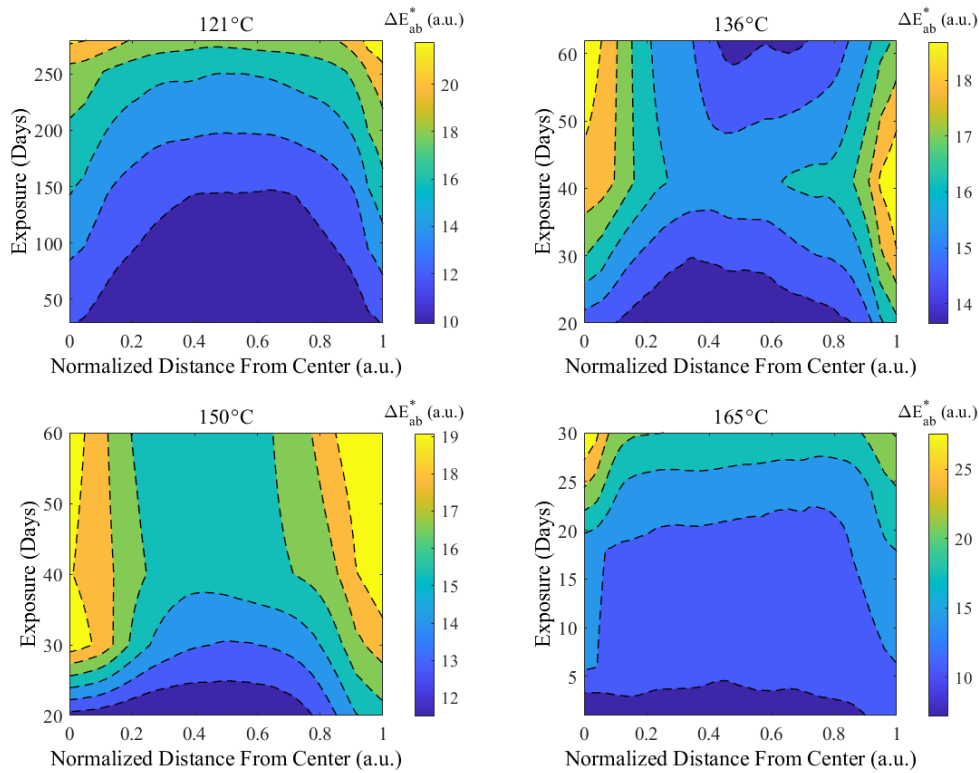
Figure 23. Three-dimensional plots of ΔE^*_{ab} as a function of exposure time (days) and normalized distance from center for specimen Rockbestos XLPE.

It is expected that the results of this work partially deviate from previous reports due to artefacts of samples harvested from active service. It is anticipated that analysis of laboratory specimens will significantly differ from commercial products due to the presence of antioxidants, inorganic additives, and processing effects on material oxygen permeability. A further effect observed in this work was the phenomenon of catalytic degradation on the interior of the cable specimen. This was most observed in specimen Anaconda EPR. This was attributed to impurities such as copper remaining from the conductor removal process [59].

41
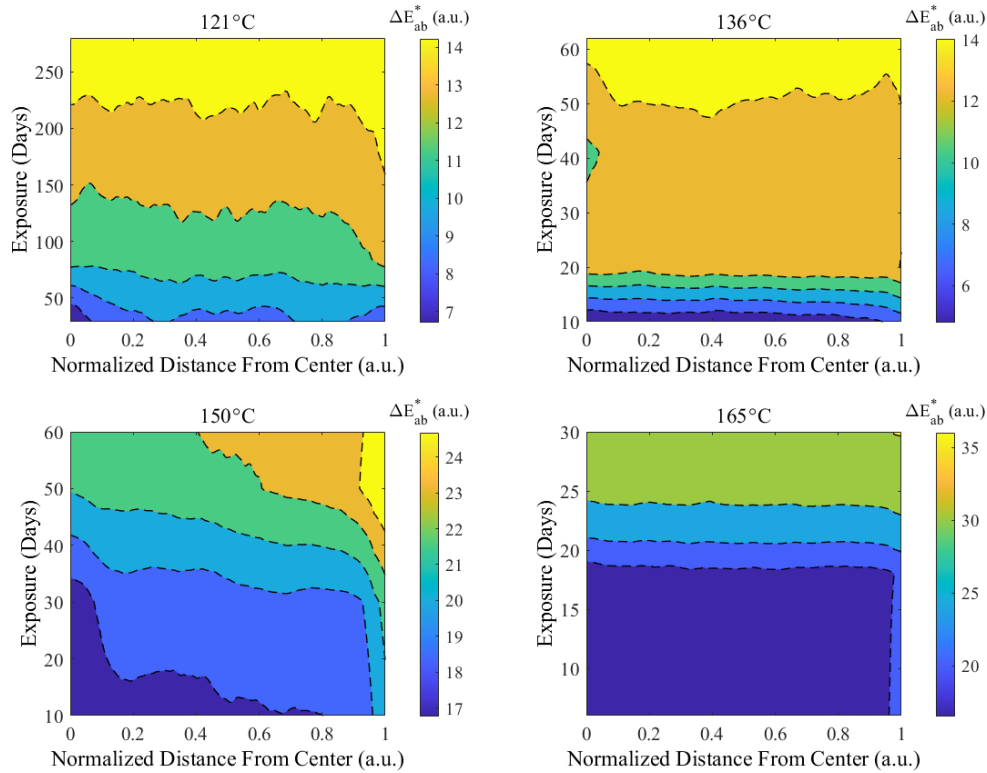
Figure 24. Three-dimensional plots of ΔE^*_{ab} as a function of exposure time (days) and normalized distance from center for specimen Brand Rex XLPE.

7.3 DLO Onset Based upon Temperature

Previous research has confirmed that the onset of DLO occurs at a given temperature and increases in magnitude as temperature increases for each polymer type [49]. Herein, we observed that Anaconda EPR followed this trend (Figure 25). However, specimen Rockbestos XLPE displayed a temperature independent DLO positive response at all investigated temperatures (Figure 25). Interestingly, specimen Brand Rex XLPE displayed a temperature independent DLO negative response although its polymer matrix is chemically similar (Figure 25). This underscores the unique behavior of each material based on its formulation and processing conditions.
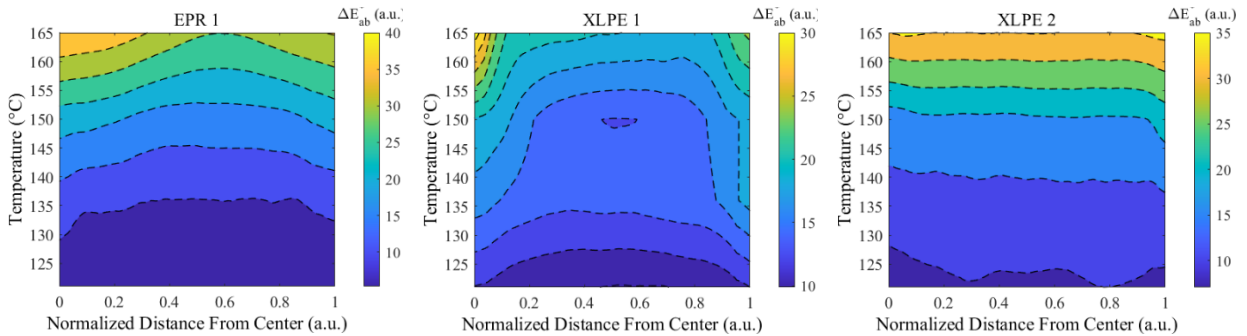
Figure 25. Three-dimensional plots of ΔE^*_{ab} as a function of exposure temperature (°C) at approximately 30 days and normalized distance from center for specimens a) Anaconda EPR, b) Rockbestos XLPE, and c) Brand Rex XLPE.

Table 12. E_a as calculated from EAB results.

Materials	E_a					
	50% absolute (kJ/mol)	50% absolute (eV)	60% retention (kJ/mol)	60% retention (eV)	50% retention (kJ/mol)	50% retention (eV)
Anaconda EPR	117.3 ± 3.6	1.21 ± 0.03	110.1 ± 8.6	1.14 ± 0.08	112.2 ± 7.1	1.16 ± 0.07
Rockbestos XLPE	109.7 ± 6.3	1.13 ± 0.06	109.6 ± 10.8	1.13 ± 0.10	109.6 ± 9.8	1.13 ± 0.10
Brand Rex XLPE	101.5 ± 6.7	1.05 ± 0.06	101.5 ± 12.4	1.05 ± 0.12	101.4 ± 13.4	1.04 ± 0.13

7.4 Comparison of Material Qualification Methods Considering DLO Effects

Activation energies (E_a) of the investigated specimens were calculated using EAB and ΔE^*_{ab} results. The superposition principle was used to generate master curves with 121 °C as the reference temperature. Shift factors were plotted against 1/T to determine E_a. Generated master curves were reported in Figures A8 and Figure A9. Activation energies were calculated using data from EAB experiments (Table 12) and from total color change (Table 13) where average ΔE^*_{ab} was calculated across the entire specimen cross section. It was expected that E_a calculations from EAB, which has been reported to not be sensitive to DLO effects, would significantly differ from E_a values calculated from ΔE^*_{ab}, which is sensitive to DLO. When DLO is important any measurement that averages across the cross section of the specimen will average oxidized and non-oxidized areas.

It was observed for specimen Anaconda EPR that the E_a value calculated from EAB results at 50% retention (112.2 ± 7.1 kJ/mol) was more conservative than the value obtained from ΔE^*_{ab} (138 ± 19 kJ/mol). It is worth mentioning that the increase in E_a is slight especially when considering the considerable error in the calculation from ΔE^*_{ab}. This difference in obtained E_a values was attributed to the significant dependence of specimen Anaconda EPR on time and temperature regarding degradation of the material. Since EAB primarily tests the surface of the material, the development of DLO accelerates material failure and reduces expected lifetimes. ΔE^*_{ab} analysis, however, considers portions of the cable insulation cross-section that have not been as heavily oxidized which results in higher E_a values.

In contrast, specimen Rockbestos XLPE was observed to exhibit lower E_a values from ΔE^*_{ab} analysis (78 ± 12 kJ/mol) than that obtained from EAB analysis (109.6 ± 9.8 kJ/mol). This difference in obtained E_a values was attributed to the mechanism of DLO observed in this specimen. Sample Rockbestos XLPE exhibited DLO only on the extreme edges of specimens, and the magnitude of the DLO and its ingress into the thickness of the specimen appeared independent of time or temperature at the conditions tested. Because the ΔE^*_{ab} method for calculating E_a uses the average total color difference value the extreme edges of specimens were averaged out. Therefore, although DLO was observed in Rockbestos XLPE specimens the calculations for E_a reduced its significance. This specimen is therefore a good example of what occurs if DLO is not accounted for when using an analytical technique that is sensitive to DLO. Finally, specimen Brand Rex XLPE was calculated to have similar E_a values calculated from EAB and ΔE^*_{ab} (101.4 ± 13.4 kJ/mol and 121 ± 18 kJ/mol, respectively). This result was attributed to the lack of DLO in the sample.

Table 13. E_a as calculated from ΔE^*_{ab} at endpoints corresponding to 50% retention of EAB.

Materials	E_a (kJ/mol)	E_a (eV)
Anaconda EPR	138 ± 19	1.43 ± 0.20
Rockbestos XLPE	78 ± 12	0.81 ± 0.12
Brand Rex XLPE	121 ± 18	1.25 ± 0.19

The primary goal of this work was to investigate whether DLO significantly affected lifetime prediction of NPP electrical cable insulation. To achieve this, E_a was calculated using a method that is known to be insensitive to DLO (EAB [60]) and using a method that was expected to be sensitive to DLO (ΔE^*_{ab}). Based on the above results, it is concluded that samples with DLO exhibit significantly different E_a values DLO is accounted for in the analytical technique. However, how that difference manifests as unique as each specimen's material chemistry, formulation, and preparation method. In the case of Anaconda EPR where the observed DLO was time and temperature dependent EAB proved to be a more conservative method of E_a calculation. However, in the case of Rockbestos XLPE where DLO was time and temperature independent E_a calculated from EAB was less conservative than that calculated by ΔE^*_{ab}. Importantly, when DLO was not observed (specimen Brand Rex XLPE) the two E_a values were within their levels of uncertainty.

An important point of discussion is the impact that specimens which were harvested from the field would have on the results presented herein. Many research efforts have used idealized materials and conditions to study the DLO phenomenon. This permits researchers to tightly control the conditions of their experiments. However, this does not account for the in-service performance for these materials and does not highlight the unique behavior of DLO attributed to sample chemical identity, formulation, and processing conditions. Furthermore, whereas idealized samples provide valuable theoretical insights into DLO, these insights are not necessarily observed outside of laboratory conditions. Finally, although the samples used in this work were harvested after a modest service life which could have influenced material response to the accelerated aging performed herein, all data was normalized to the as-received samples to minimize any such effects. In conclusion, the results of this work suggest that DLO has an adverse effect on E_a calculations and cable insulation lifetime predictions. In addition, specific conclusions regarding the adverse effect of DLO on material qualification studies require additional investigation for each unique material as the effect of polymer chemistry, additives in the formulation, and processing conditions are not negligible.

8.   CONCLUSIONS

Nuclear cable insulation samples of the two most common types, EPR and XPLE, from three of the most sourced manufacturers, Anaconda, Rockbestos and Brand-Rex, were subjected to thermal aging at temperatures like those used in historic environmental qualification, 121, 136, 150, and 165 °C. The aged materials were characterized for effects of aging using the conventional tensile EAB for all three and indenter modulus for the EPR. Cross-sections of the aged insulation were further examined for evidence of inhomogeneous aging through the thickness of the material using the previously reported techniques of nano-indentation, SEM-EDS, and FTIR, as well as a new technique for tracking location specific aging—total color change.

Cable cross-sections from each material at each aging temperature and for a series of aging durations were imaged and analyzed for total color change versus each as-received material. Overall color change was observed to track with exposure severity. Inhomogeneous color change, manifest as increased color change near the inner and outer edges of the insulation, were observed. The inhomogeneous aging behavior was seen to vary among the three materials, being most prominent and temperature dependent in the Anaconda EPR material, present at all temperatures but edge restricted in the Rockbestos XLPE material, and not evident in the Brand Rex XLPE material. Oxidation was confirmed as the source of the outer edge inhomogeneous color change in nano-indentation, EDS and FTIR results, as expected. Aging at the interior edge of the insulation was also seen to be extremely material dependent, being greatest in the Anaconda EPR, less evident in Rockbestos XLPE and not evident in Brand Rex XLPE. The exterior inhomogeneous oxidation behavior is understood to result from classic diffusion limited oxidation, but the interior degradation abnormality is thought to be related to contact of the insulation with conductor materials such a copper-ion catalyzed oxidation.

An identified concern for cable aging management in long-term operation is that inhomogeneous aging such as DLO due to the extreme conditions of accelerated aging may not be representative of service aging and may not be sufficiently conservative. If DLO shields insulation from aging at higher temperatures, extrapolation of that degradation to lower service temperatures may lead to overestimation of viable insulation service life.

In this report, activation energy values were calculated for the three materials using the traditional EAB method, that is thought to be insensitive to DLO. Activation energy values were also calculated from the average total color change values of each material, data that is affected by the DLO. It was found that the activation energy calculated from total color change for Anaconda EPR, for which DLO was strongly observed, was slightly higher than the E_a calculated from EAB. That is, the EAB prediction was slightly more conservative: 19% lower E_a for EAB than for ΔE^*_{ab}, plus/minus 14%. For the Rockbestos XLPE considered, in which DLO was observed at all temperatures considered, the EAB-derived E_a was found to be higher by 40% plus/minus 15%. For the Brand Rex XLPE material considered, in which no DLO was observed, the EAB- and ΔE^*_{ab}-derived E_a values were found to be very similar, 17% plus/minus 15% greater for ΔE^*_{ab}.

DLO was found to affect calculated E_a values by a degree that differed by material. Uncertainty in the values calculated from the methods examined led to similar results between metrics thought to be DLO-affected and not DLO-affected. Total color change was determined to be a useful and effective way to quantify location-specific aging that is quick and convenient. The conclusions that can be drawn from this work are limited by the materials and conditions (temperatures) explored, but also by the state of the material available (varies levels of service aging, material thickness, material shape). It appeared evident, especially in the Anaconda EPR material studied, that the materials in contact with the insulation during prior service strongly affected the material aging (such as copper-catalyzed oxidation). Further research to understand the impact of inhomogeneous aging on SLR-relevant cable aging management would benefit from application of the techniques developed in this work to 1) additional cable materials, 2) insulation samples of various thicknesses available in sufficient quantity and form for oxygen permeation testing, and 3) investigation of cable inhomogeneous aging of non-DLO origin such as copper-catalyzed oxidation and diffusion of chloride, antimony and other species from flame retardant jacket materials.

9.   REFERENCES

[1]   NRC, *Expanded Materials Degradation Assessment (EMDA), Volume 1: Executive Summary of EMDA Process and Results*, NUREG/CR-7153, U.S. Nuclear Regulatory Commission, 2013.

[2]   P.L. Joskow, *The Future of nuclear power in the United States: Economic and regulatory challenges*, MIT-CEEPR 06-019WP, MIT Center for Energy and Env. Policy Research, 2006.

[3]   NRC, *Literature Review of Environmental Qualification of Safety-Related Electric Cables*, NUREG/CR-6384 (BNL-NUREG-52840), U.S. Nuclear Regulatory Commission, 1996.

[4]   SNL, *Aging Management Guideline for Commercial Nuclear Power Plants Electrical Cable and Terminations*, SAND96-0344, Sandia National Laboratories, 1996.

[5]   NRC, *Expanded Materials Degradation Assessment (EMDA), Volume 5: Aging of Cables and Cable Systems*, NUREG/CR-7153, U.S. Nuclear Regulatory Commission, 2014.

[6]   NEA, *Cable Ageing in Nuclear Power Plants*, NEA/CSNI/R(2018)8, Nucl. Energy Agency, 2018.

[7]   PNNL, *Light Water Reactor Sustainability (LWRS) Program–Non-Destructive Evaluation (NDE) R&D Roadmap for Determining Remaining Useful Life of Aging Cables in Nuclear Power Plants,* PNNL-21731, Pacific Northwest National Laboratory, 2012.

[8]   PNNL, *Initiation of Experimental Campaign to Address Knowledge Gaps Related to Simultaneous Thermal and Gamma Radiation Aging of Crosslinked Polyethylene and Ethylene-Propylene Rubber Cable Insulation*, PNNL-27987, Pacific Northwest National Laboratory, 2018.

[9]   K.T. Gillen, R.L. Clough, Rigorous experimental confirmation of a theoretical model for diffusion-limited oxidation, *Polymer*. 33(20), 4358–4365 (1992). doi.org/10.1016/0032-3861(92)90280-A.

[10]   L. Verardi, D. Fabiani, G.C. Montanari, Correlation of electrical and mechanical properties in accelerated aging of LV nuclear power plant cables, *ICHVE 2014 - 2014 International Conference on High Voltage Engineering and Application*. 1–4 (2014).doi.org/10.1109/ICHVE.2014.7035376.

[11]   K.T. Gillen, R.L. Clough, "Time-temperature-dose rate superposition: A methodology for extrapolating accelerated radiation aging data to low dose rate conditions", *Polymer Degradation and Stability*. 24 137–168 (1989). doi.org/10.1016/0141-3910(89)90108-0.

[12]   G. Przybytniak, J. Boguski, V. Placek, L. Verardi, D. Fabiani, E. Linde, U.W. Gedde, "Inverse effect in simultaneous thermal and radiation aging of EVA insulation", *Express Polymer Letters*. 9 384–393 (2015). doi.org/10.3144/expresspolymlett.2015.36.

[13]   K.T. Gillen, "Importance of Synergism for Degradation of Elastomers in Combined Radiation Plus Temperature Environments", *Rubber Chemistry and Technology*. 93 121–141 (2019). doi.org/10.5254/rct.19.80457.

[14]   T. Seguchi, K. Tamura, T. Ohshima, A. Shimada, H. Kudoh, "Degradation mechanisms of cable insulation materials during radiation-thermal ageing in radiation environment", *Radiation Physics and Chemistry*. 80 268–273 (2011). doi.org/10.1016/j.radphyschem.2010.07.045.

[15]   M.C. Celina, A.R. Dayile, A. Quintana, A perspective on the inherent oxidation sensitivity of epoxy materials, *Polymer*. 54 3290–3296 (2013). doi.org/10.1016/j.polymer.2013.04.042.

[16]   K. T. Gillen, R.A. Assink, and R. Bernstein, *Nuclear Energy Plant Optimization (NEPO): Final Report on Aging and Condition Monitoring of Low-Voltage Cable Materials*, SAND2005-7331 (EPRI 1011873), Sandia National Laboratories, 2005.

[17]   PNNL, *Initial Evaluations of Effects of Diffusion Limited Oxidation (DLO) Testing,* PNNL-28351, Pacific Northwest National Laboratory, 2018.

[18]   SNL, *Aging Management Guideline for Commercial Nuclear Power Plants Electrical Cable and Terminations*, SAND96-0344, Sandia National Laboratories, 1996.

[19]   SNL, *Aging Management Guideline for Commercial Nuclear Power Plants Electrical Cable and Terminations*, SAND96-0344, Sandia National Laboratories, 1996.

[20]   EPRI, *Low-voltage environmentally-qualified cable license renewal industry report: Revision 1. Final report*, EPRI-TR-103841, Electric Power Research Institute, 1994.

[21] P. Hu, P.P. Zhao, G.W. Zhang, X.H. Wang, "Thermal properties of 60Co irradiated crosslinked high density polyethylene", *Solar Energy Materials and Solar Cells*. 149 55–59 (2016). doi.org/10.1016/j.solmat.2015.12.042.

[22] A.R. Amin, "Synergistic effect of TNPP and carbon black in weathered XLPE materials", *Journal of Polymers and the Environment*. 17 267–272 (2009). doi.org/10.1007/s10924-009-0148-5.

[23] R. Kochetov, T. Christen, F. Gullo, "FTIR analysis of LDPE and XLPE thin samples pressed between different protective anti-Adhesive films", *ICEMPE 2017 - 1st International Conference on Electrical Materials and Power Equipment*. 49–52 (2017). doi.org/10.1109/ICEMPE.2017.7982097.

[24] Q. Zhao, X. Li, J. Gao, "Aging of ethylene-propylene-diene monomer (EPDM) in artificial weathering environment", *Polymer Degradation and Stability*. 92 1841–1846 (2007). doi.org/10.1016/j.polymdegradstab.2007.07.001.

[25] M. Tefferi, Z. Li, Y. Cao, H. Uehara, Q. Chen, "Novel EPR-insulated DC cables for future multi-terminal MVDC integration", *IEEE Electrical Insulation Magazine*. 35 20–27 (2019). doi.org/10.1109/MEI.2019.8804331.

[26] IEC/IEEE, *Nuclear power plants - Instrumentation and control important to safety - Electrical equipment condition monitoring methods - Part 3: Elongation at break*, IEC/IEEE 62582-3:2012, International Electrotechnical Commission, Institute of Electrical and Electronics Engineers, 2012.

[27] ASTM, *Standard Practice for Conditioning Plastics for Testing*, ASTM D618-13, ASTM International, 2013. doi.org/10.1520/D0618-13.

[28] L. Greenspan, "Humidity fixed points of binary saturated aqueous solutions", *Journal of Research of the National Bureau of Standards Section A: Physics and Chemistry*. 81A 89 (1977). doi.org/10.6028/jres.081A.011.

[29] ASTM, *Standard Practice for Calculation of Color Tolerances and Color Differences from Instrumentally Measured Color Coordinates*, ASTM D2244-16, ASTM International, 2016. doi.org/10.1520/D2244-16.

[30] ASTM, *Standard Practice for Visual Appraisal of Colors and Color Differences of Diffusely-Illuminated Opaque Materials*, ASTM D1729-16, ASTM International, 2016. doi.org/10.1520/D1729-16.

[31] J. Troscianko, Empirical Imaging, 2020. http://www.empiricalimaging.com/ (accessed January 23, 2020).

[32] J. Troscianko, M. Stevens, "Image calibration and analysis toolbox - a free software suite for objectively measuring reflectance, colour and pattern", *Methods in Ecology and Evolution*. 6 1320–1331, (2015). https://doi.org/10.1111/2041-210X.12439.

[33] S.A. Burns, Generating Reflectance Curves from sRGB Triplets, (2015) 1–39. scottburns.us/reflectance-curves-from-srgb/

[34] S.G. Kazarian, K.L.A. Chan, "ATR-FTIR spectroscopic imaging: Recent advances and applications to biological systems", *Analyst*. 138 1940–1951 (2013). doi.org/10.1039/c3an36865c.

[35] IEC/IEEE, *Nuclear power plants - Instrumentation and control important to safety - Electrical equipment condition monitoring methods - Part 2: Indenter modulus*, IEC/IEEE 62582-2:2011, International Electrotechnical Commission, Institute of Electrical and Electronics Engineers, 2011.

[36] Y. Zhang, Z. Wu, C. Qian, X. Tan, J. Yang, L. Zhong, "Research on lifespan prediction of cross-linked polyethylene material for XLPE cables", *Applied Sciences* (Switzerland). 10 (2020). doi.org/10.3390/APP10155381.

[37] K.T. Gillen, M. Celina, R. Bernstein, "Validation of improved methods for predicting long-term elastomeric seal lifetimes from compression stress-relaxation and oxygen consumption techniques", *Polymer Degradation and Stability*. 82 25–35 (2003). doi.org/10.1016/S0141-3910(03)00159-9.

[38] K.T. Gillen, R. Bernstein, M. Celina, "Non-Arrhenius behavior for oxidative degradation of chlorosulfonated polyethylene materials", *Polymer Degradation and Stability*. 87 335–346 (2005). https://doi.org/10.1016/j.polymdegradstab.2004.09.004.

[39] M.C. Celina, "Review of polymer oxidation and its relationship with materials performance and lifetime prediction", *Polymer Degradation and Stability*. 98 2419–2429 (2013). doi.org/10.1016/J.POLYMDEGRADSTAB.2013.06.024.

[40] L. Boukezzi, A. Boubakeur, C. Laurent, M. Lallouani, "Observations on Structural Changes under Thermal Ageing of Cross-linked Polyethylene Used as Power Cables Insulation", *Iranian Polymer Journal (English),* 17(8) 611-624 (2008).

[41] Y. Zhang, Z. Hou, K. Wu, S. Wang, J. Li, S. Li, "Influence of oxygen diffusion on thermal ageing of cross-linked polyethylene cable insulation", *Materials*, *13*(9), 205613 (2020). doi.org/10.3390/MA13092056.

[42] Y. Kemari, A. Mekhaldi, G. Teyssedre, M. Teguar, "Correlations between structural changes and dielectric behavior of thermally aged XLPE", *IEEE Transactions on Dielectrics and Electrical Insulation*. 26 1859–1866 (2019). doi.org/10.1109/TDEI.2019.008189.

[43] X. Yang, Y. Zhang, H. He, M. Qiu, X. Yu, J. Li, "Influence of Thermal Ageing on the Optical Performance of XLPE Cable Insulation", *2020 International Symposium on Electrical Insulating Materials (ISEIM)*, 2020.

[44] L.S. Fifield, Y. Shin, K.L. Simmons, "Non-destructive evaluation of polyolefin thermal aging using infrared spectroscopy", in: *Nondestructive Characterization and Monitoring of Advanced Materials, Aerospace, and Civil Infrastructure 2017*, SPIE, 2017: p. 101690U. doi.org/10.1117/12.2261983.

[45] G. Gryn'ova, J.L. Hodgson, M.L. Coote, "Revising the mechanism of polymer autooxidation, Organic and Biomolecular Chemistry", 9 480–490 (2011). doi.org/10.1039/c0ob00596g.

[46] X. Colin, J. Verdu, "Strategy for studying thermal oxidation of organic matrix composites", *Composites Science and Technology*. 65 411–419 (2005). doi.org/10.1016/j.compscitech.2004.09.011.

[47] E. Linde, F. Nilsson, M. Barrett, M.S. Hedenqvist, M.C. Celina, "Time- and Feedback-Dependent DLO Phenomena in Oxidative Polymer Aging", *Polymer Degradation and Stability*. 189 (2021). doi.org/10.1016/j.polymdegradstab.2021.109598.

[48] A. Quintana, M.C. Celina, Overview of DLO modeling and approaches to predict heterogeneous oxidative polymer degradation, Polymer Degradation and Stability. 149 (2018) 173–191. doi.org/10.1016/j.polymdegradstab.2017.11.014.

[49] J. Wise, K.T. Gillen, R.L. Clough, "Quantitative model for the time development of diffusion-limited oxidation profiles", *Polymer*. 38(8) 1929-1944 (1997). doi.org/10.1016/S0032-3861(96)00716-1.

[50] P.Y. Le Gac, M. Celina, G. Roux, J. Verdu, P. Davies, B. Fayolle, "Predictive ageing of elastomers: Oxidation driven modulus changes for polychloroprene", *Polymer Degradation and Stability*. 130 (2016) 348–355. doi.org/10.1016/j.polymdegradstab.2016.06.014.

[51] J. Zhao, R. Yang, R. Iervolino, S. Barbera, "Changes of chemical structure and mechanical property levels during thermo-oxidative aging of NBR", *Rubber Chemistry and Technology*. 86 591–603 (2013). doi.org/10.5254/RCT.13.87969.

[52] Y. Wang, M. Gupta, D.A. Schiraldi, "Oxygen permeability in thermoplastic polyurethanes", *Journal of Polymer Science, Part B: Polymer Physics*. 50 681–693 (2012). doi.org/10.1002/polb.23053.

[53] S. Chowdhury, V.R. Bhethanabotla, R. Sen, "Measurement of oxygen diffusivity and permeability in polymers using fluorescence microscopy", *Microscopy and Microanalysis*. 16(6) 725–734. doi.org/10.1017/S1431927610000401.

[54] M. Celina, K.T. Gillen, "Superposition and wear-out approaches applied to polymer lifetime prediction", Polymer Preprints, 42(1) (2001). SAND2000-3036C.

[55] SNL, *Nuclear Power Plant Cable Materials : Review of Qualification and Currently Available Aging Data for Margin Assessments in Cable Performance*. SAND2013-2388, Sandia National Laboratories, 2013. doi.org/10.2172/1096518.

[56] K.T. Gillen, R.L. Clough, C.A. Quintana, "Modulus Profiling of Polymers", *Polymer Degradation and Stability*. 17(1) 31-47 (1987). doi.org/10.1016/0141-3910(87)90046-2.

[57] R.L. Clough, K.T. Gillen, C.A. Quintana, "Heterogeneous oxidative degradation in irradiated polymers", *Journal of Polymer Science: Polymer Chemistry Edition*. 23 359–377 (1985). doi.org/10.1002/pol.1985.170230212.

[58] K.T. Gillen, R.L. Clough, N.J. Dhooge, "Density profiling of polymers", *Polymer.* 27(2) 225-232 (1986). doi.org/10.1016/0032-3861(86)90330-7.

[59] J. Li, H. Li, F. Zhou, S. Wang, J. Zhao, B. Ouyang, "Copper-catalyzed oxidation caused by copper-rich impurities in cross-linked polyethylene cable insulation", *Journal of Materials Science: Materials in Electronics*. 27 806–810 (2016). doi.org/10.1007/s10854-015-3820-7.

[60] J. Wise, K.T. Gillen, R.L. Clough, "An ultrasensitive technique for testing the Arrhenius extrapolation assumption for thermally aged elastomers", *Polymer Degradation and Stability*. 49 403–418 (1995). doi.org/10.1016/0141-3910(95)00137-B.

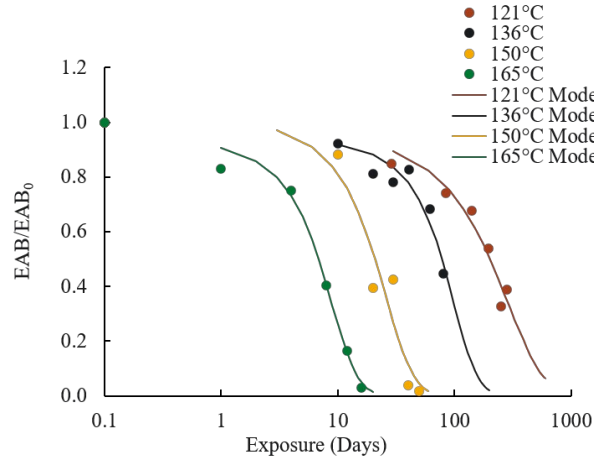# 10. APPENDIX

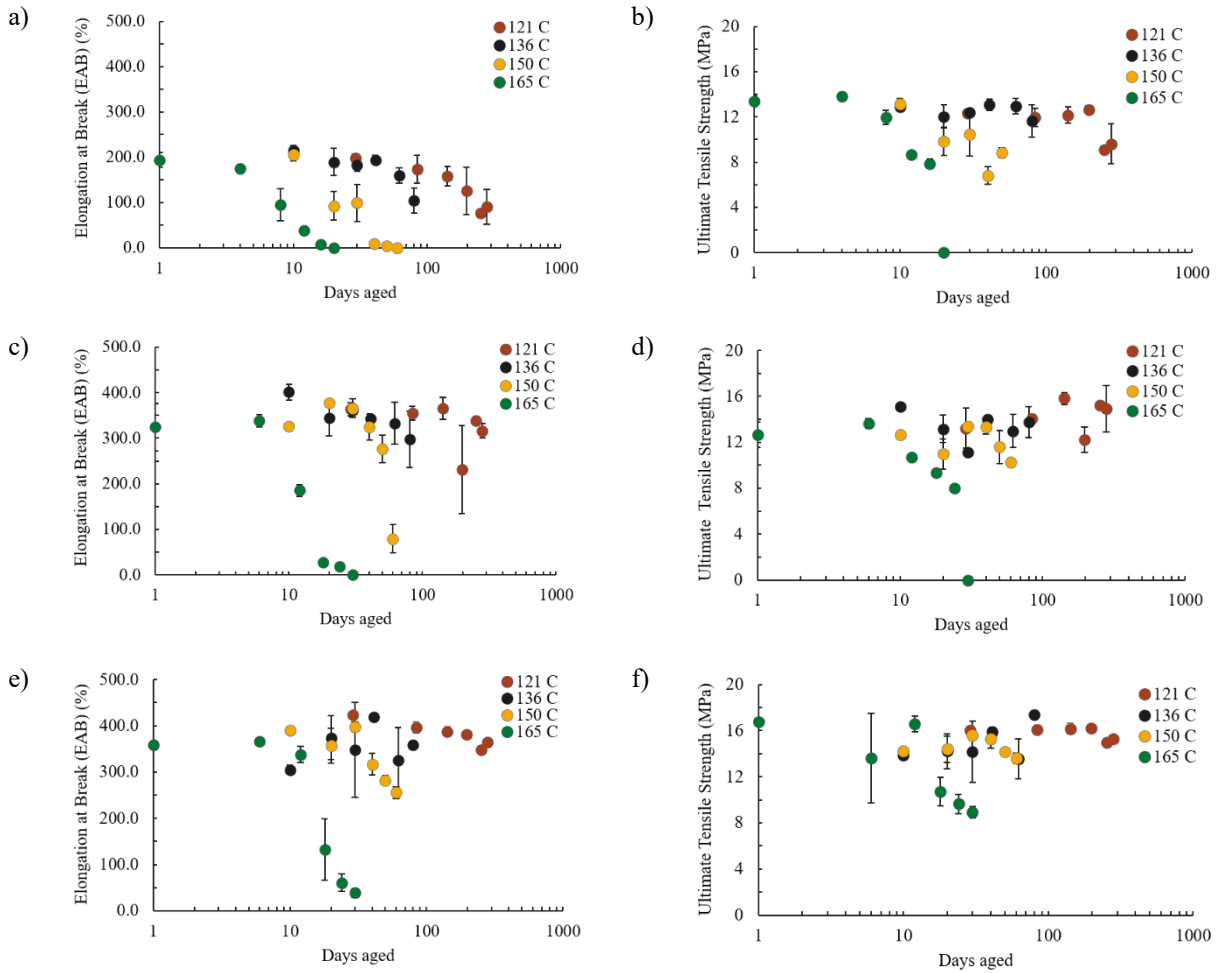Figure A1. Visual depiction of sigmoidal fit to EAB data used to generate 50% retention thresholds.

Figure A2. Complete obtained results from EAB and ultimate tensile strength analyses of cable specimens. a) Anaconda EPR EAB results b) Anaconda EPR UTS results c) Rockbestos XLPE EAB results d) Rockbestos XLPE UTS results e) Brand Rex XLPE EAB results and f) XLPE UTS results.

50

Table A1. Individual specimen calculations used to generate DLO thresholds for specimen Anaconda EPR

Temperature (°C)	Aging duration	ΔE*ab at center	ΔE*ab at 0.05 normalized distance from center	ΔE*ab % change from center to inside edge	ΔE*ab at 0.95 normalized distance from center	ΔE*ab % change from center to outside edge
121	29	5.5	5.8	5 %	5.6	2 %
	84	10.5	12.7	21 %	11.3	7 %
	142	12.0	15.4	28 %	13.4	11 %
	197	14.2	17.7	24 %	15.3	7 %
	252	13.2	17.1	29%	15.2	15%
	280	15.0	19.1	27 %	14.7	2 %
136	10	7.2	9.5	30 %	8.7	19 %
	20	11.0	13.4	22 %	11.9	9 %
	30	9.9	11.3	14 %	11.0	11 %
	41	11.3	13.7	22 %	13.0	15 %
	62	10.6	14.4	36 %	12.2	15 %
	80	14.5	18.0	24 %	15.7	8 %
150	10	13.0	17.3	33 %	15.4	18 %
	20	15.9	21.3	34 %	18.1	14 %
	30	18.0	22.1	23 %	21.7	20 %
	40	22.1	34.4	56 %	23.2	5 %
165	1	7.2	9.8	37 %	9.6	33 %
	4	14.6	17.3	18 %	16.5	13 %
	8	17.4	20.3	17 %	18.2	5 %
	12	17.5	28.1	60 %	19.1	9 %

Table A2. Individual specimen calculations used to generate DLO thresholds for specimen Rockbestos XLPE

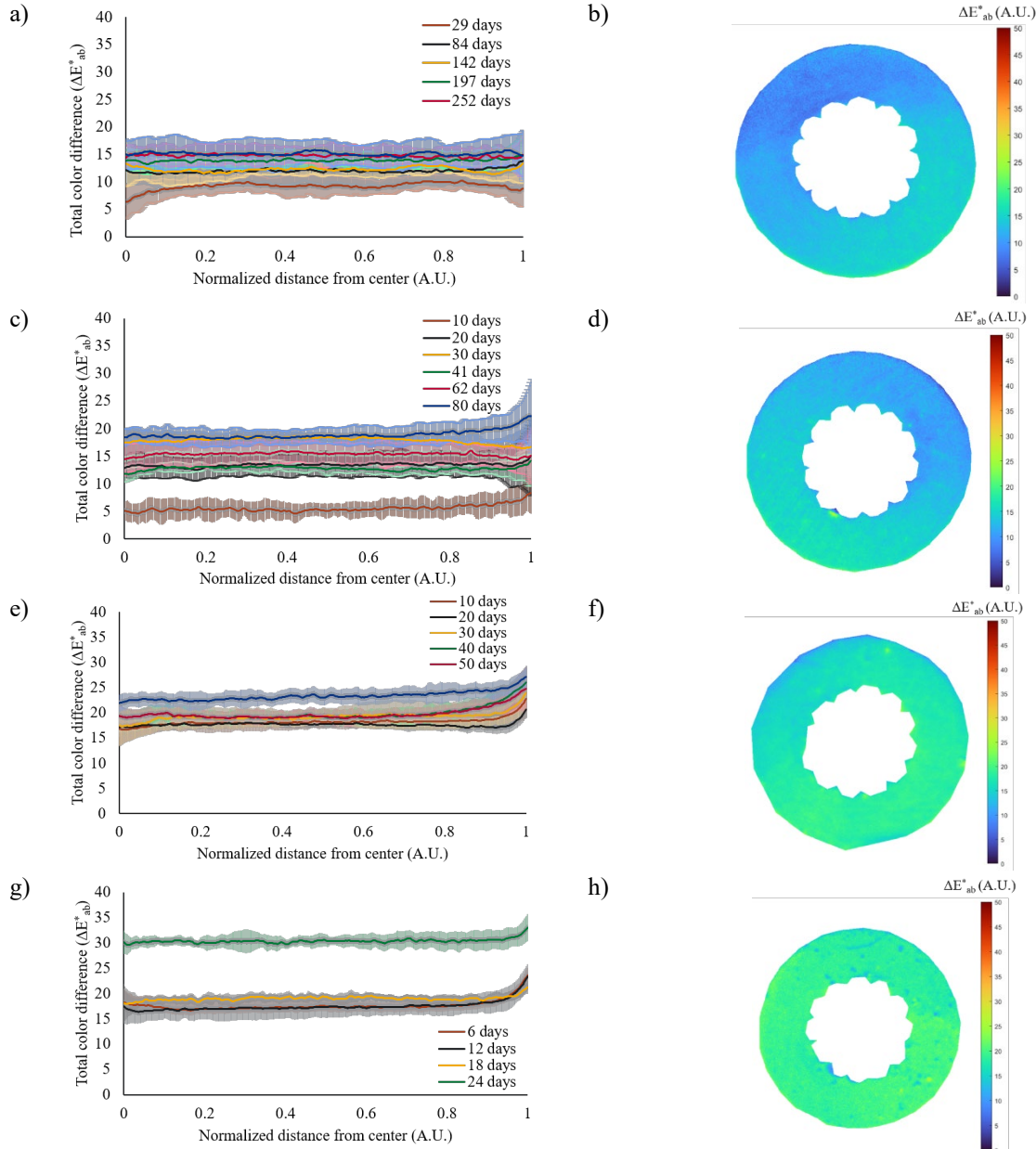| Temperature (°C)	Aging duration	ΔE^*_{ab} at center	ΔE^*_{ab} at 0.05 normalized distance from center	ΔE^*_{ab} % change from center to inside edge	ΔE^*_{ab} at 0.95 normalized distance from center	ΔE^*_{ab} % change from center to outside edge
121	29	9.9	11.7	18%	11.3	14%
	84	14.8	16.3	10%	16.0	7%
	142	11.8	15.2	29%	15.1	28%
	197	15.8	18.8	19%	17.0	8%
	252	15.9	18.7	18%	19.7	24%
	280	18.3	21.9	19%	22.2	21%
136	10	17.2	18.0	5%	20.6	19%
	20	13.8	14.8	7%	16.0	16%
	30	14.7	16.7	13%	17.8	20%
	41	16.0	18.4	15%	18.8	17%
	62	14.2	18.8	32%	16.6	16%
	80	14.6	17.3	18%	19.8	35%
150	10	10.4	12.0	16%	13.3	29%
	20	11.6	12.2	6%	16.1	39%
	30	14.0	20.2	44%	18.2	30%
	40	15.9	19.2	21%	19.8	25%
	50	13.1	17.1	31%	19.3	48%
	60	15.9	19.3	21%	20.4	28%
165	1	9.5	7.6	20%	11.7	24%
	6	11.2	13.7	22%	13.2	18%
	12	14.8	15.0	1%	16.6	13%
	18	12.6	14.3	13%	16.7	32%

Figure A3. Total color difference (ΔE^*_{ab}) plots and surface images of specimens a) compiled ΔE^*_{ab} plots for Brand Rex XLPE specimens aged at 121 °C b) ΔE^*_{ab} surface plot of Brand Rex XLPE aged at 121 °C for 29 days c) compiled ΔE^*_{ab} plots for Brand Rex XLPE specimens aged at 136 °C d) ΔE^*_{ab} surface plot of Brand Rex XLPE aged at 136 °C for 20 days e) compiled ΔE^*_{ab} plots for Brand Rex XLPE specimens aged at 150 °C f) ΔE^*_{ab} surface plot of Brand Rex XLPE aged at 150 °C for 20 days g) compiled ΔE^*_{ab} plots for Brand Rex XLPE specimens aged at 165 °C h) ΔE^*_{ab} surface plot of Brand Rex XLPE aged at 165 °C for 18 days.

Table A3. Individual specimen calculations used to generate DLO thresholds for specimen Brand Rex XLPE

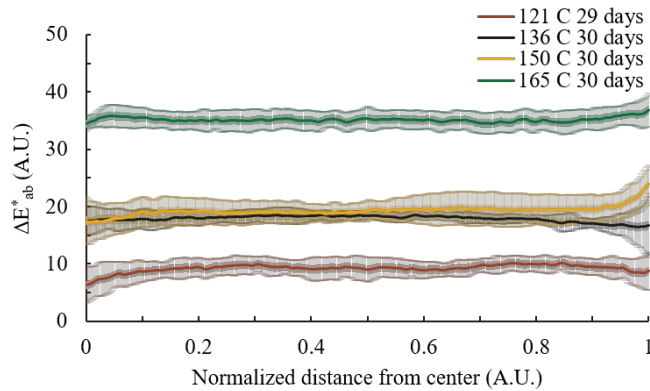| Temperature (°C)	Aging duration	ΔE^*_{ab} at center	ΔE^*_{ab} at 0.5 normalized distance from center	ΔE^*_{ab} % change from center to inside edge	ΔE^*_{ab} at 0.95 normalized distance from center	ΔE^*_{ab} % change from center to outside edge
121	29	9.2	8.0	13%	9.2	1%
	84	12.0	11.7	3%	12.7	6%
	142	12.3	12.5	2%	11.8	4%
	197	13.8	13.4	3%	14.2	3%
	252	14.7	15.0	2%	14.5	2%
	280	15.6	15.4	1%	15.5	0%
136	10	5.2	5.1	2%	6.7	29%
	20	13.5	13.3	2%	13.3	2%
	30	18.4	17.7	4%	16.8	9%
	41	12.7	12.4	3%	12.7	0%
	62	15.4	15.0	3%	14.5	6%
	80	18.8	18.6	1%	20.3	8%
150	10	18.2	17.1	6%	19.4	7%
	20	17.8	17.5	2%	17.4	2%
	30	19.3	17.9	7%	20.3	5%
	40	19.3	19.4	0%	23.1	20%
	50	22.7	21.9	3%	25.0	10%
	60	23.1	22.6	2%	25.0	8%
165	1	17.5	17.7	1%	19.5	12%
	6	17.4	16.5	5%	19.1	10%
	12	19.3	18.5	4%	19.4	1%
	18	30.5	30.1	1%	30.9	1%

Figure A4. compiled ΔE^*_{ab} plots for Brand Rex XLPE specimens aged at various temperatures but constant durations.
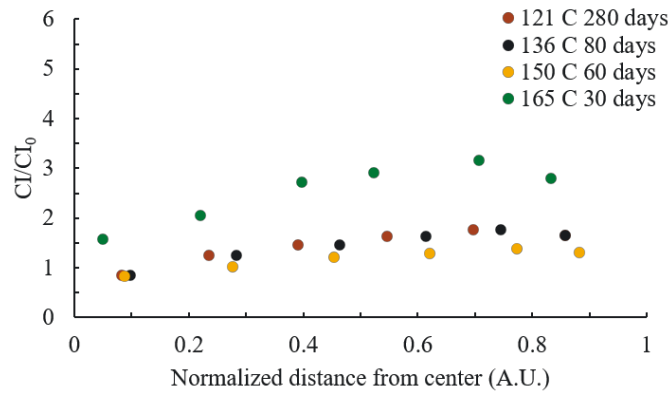
a)
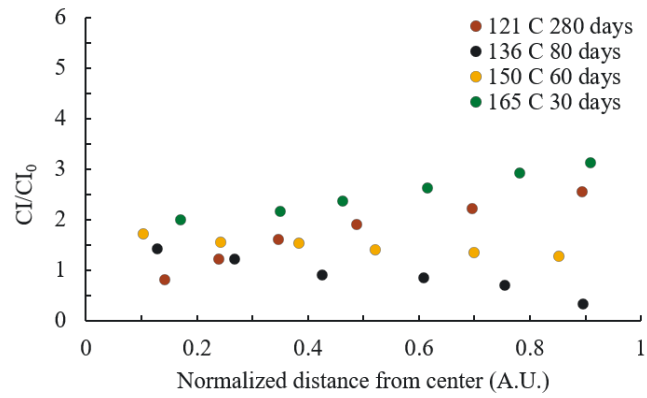
b)

Figure A5. Normalized carbonyl index (CI) of specimens a) Rockbestos XLPE aged at various temperatures and for select durations and b) Brand Rex XLPE aged at various temperatures and for select durations which were used for verification of color analysis.
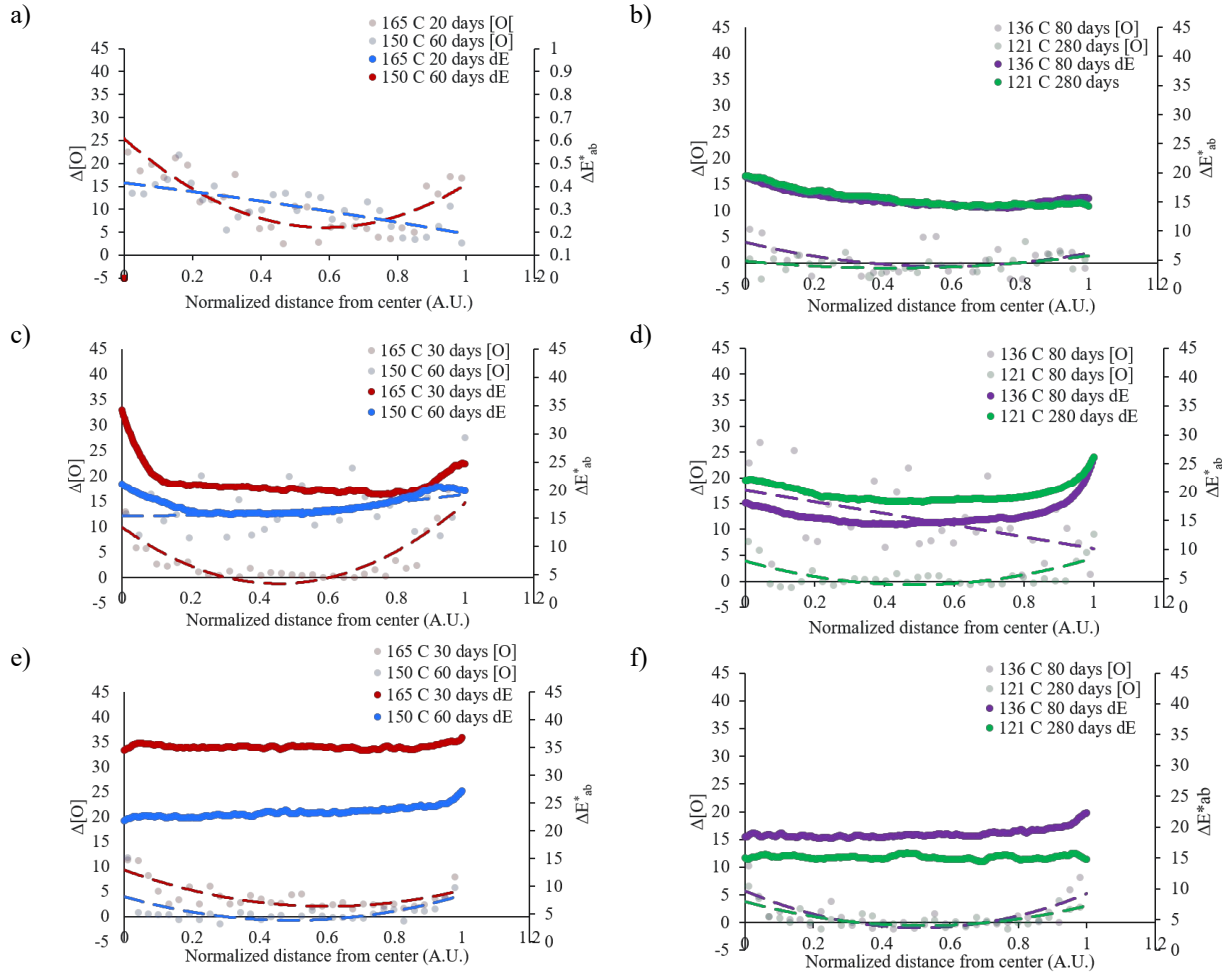
Figure A6. Additional total color difference analysis verification data where [O] is defined as oxygen concentration a) EDS and commensurate ΔE^*_{ab} results for specimen Anaconda EPR at 165 and 150 °C b) EDS and commensurate ΔE^*_{ab} results for specimen Anaconda EPR at 136 and 121 °C c) EDS and commensurate ΔE^*_{ab} results for specimen Rockbestos XLPE at 165 and 150 °C d) EDS and commensurate ΔE^*_{ab} results for specimen Rockbestos XLPE at 136 and 121 °C e) EDS and commensurate ΔE^*_{ab} results for specimen Brand Rex XLPE at 165 and 150 °C f) EDS and commensurate ΔE^*_{ab} results for specimen Brand Rex XLPE at 136 and 121 °C.
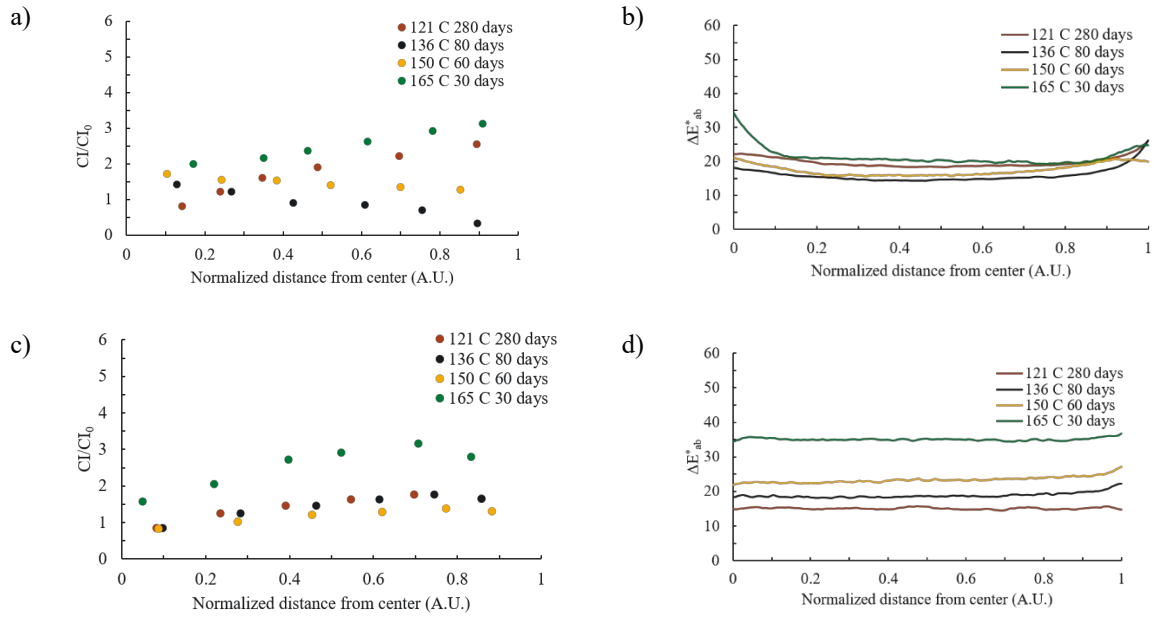
Figure A7. a) normalized carbonyl index (CI) results of specimen Rockbestos XLPE aged at various temperatures and for select durations used for ΔE^{*}_{ab} comparisons b) ΔE^{*}_{ab} results of specimen Brand Rex XLPE commensurate to adjacent CI plot c) normalized carbonyl index (CI) results of specimen Brand Rex XLPE aged at various temperatures and for select durations used for ΔE^{*}_{ab} comparisons d) ΔE^{*}_{ab} results of specimen Brand Rex XLPE commensurate to adjacent CI plot.
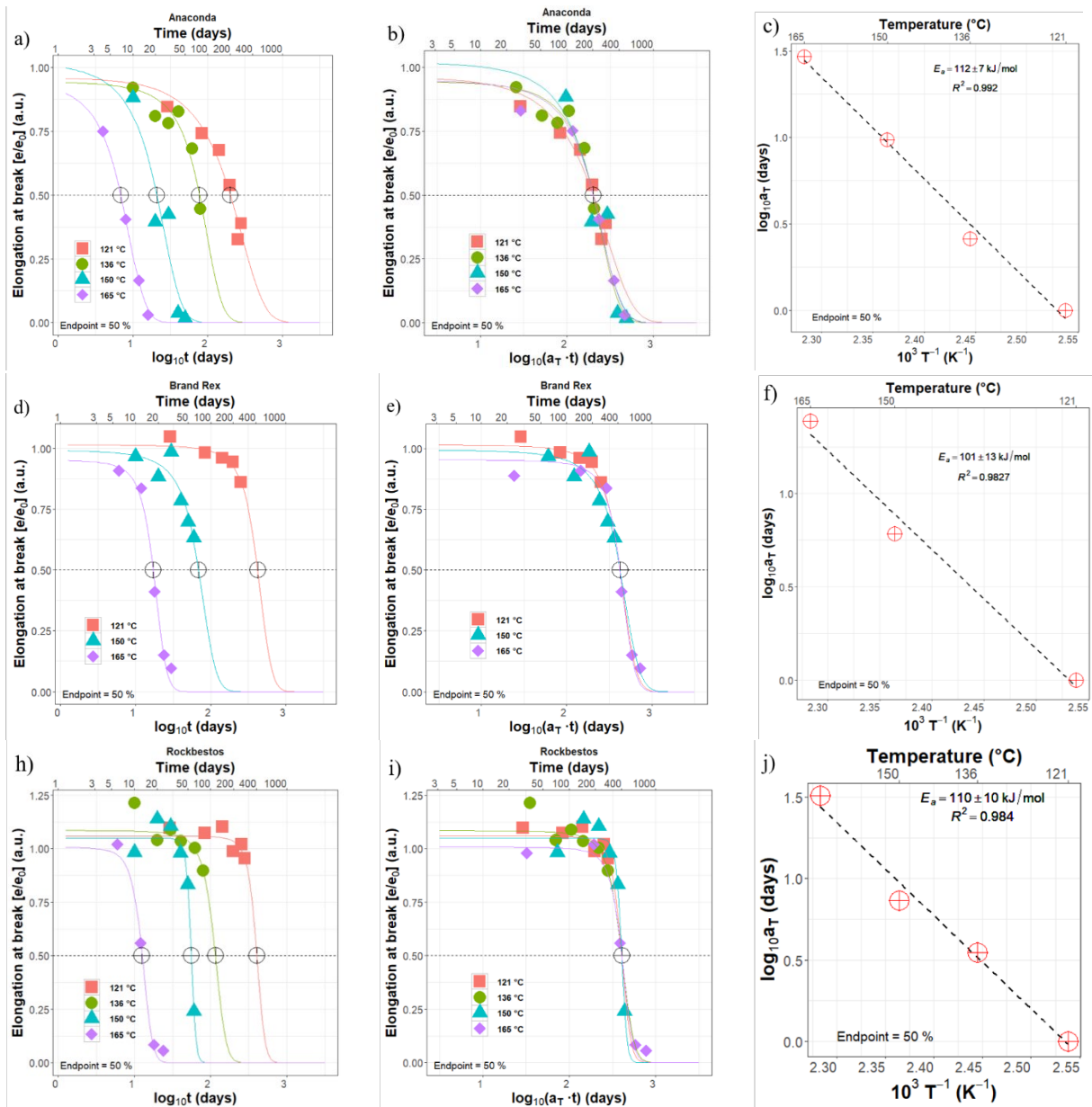
Figure A8. a) plotted EAB results of specimen Anaconda EPR with sigmoidal line of best fit b) superimposed EAB results of specimen Anaconda EPR with sigmoidal line of best fit c) shift factor of superimposed Anaconda EPR EAB results plotted against temperature used to calculate E_a d) plotted EAB results of specimen Rockbestos XLPE with sigmoidal line of best fit e) superimposed EAB results of specimen Rockbestos XLPE with sigmoidal line of best fit f) shift factor of superimposed Rockbestos XLPE EAB results plotted against temperature used to calculate E_a h) plotted EAB results of specimen Brand Rex XLPE with sigmoidal line of best fit i) superimposed EAB results of specimen Brand Rex XLPE with sigmoidal line of best fit j) shift factor of superimposed Brand Rex XLPE EAB results plotted against temperature used to calculate E_a.
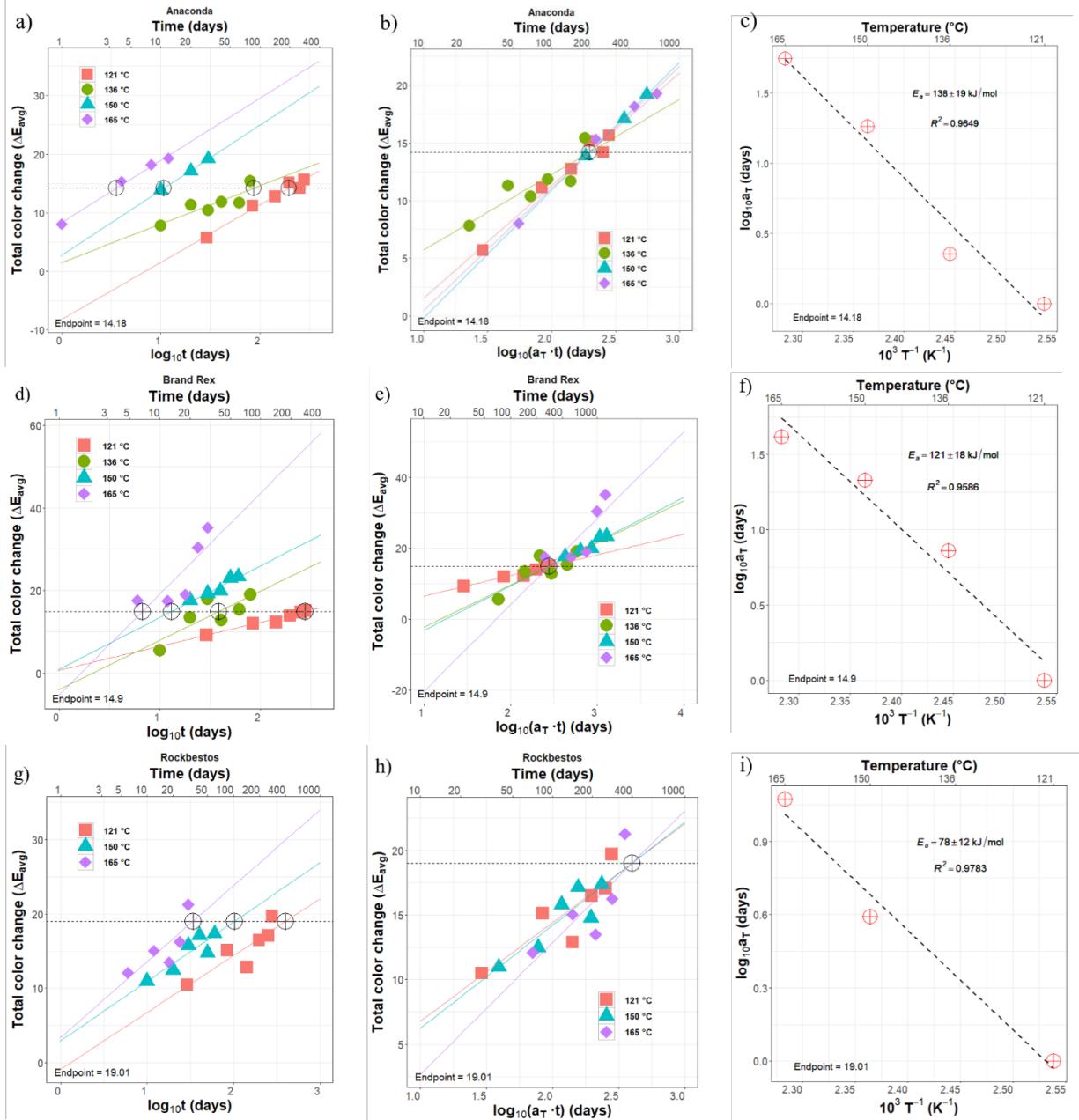
Figure A9. a) plotted average ΔE^*_{ab} as a function of aging temperature and duration for specimen Anaconda EPR with a linear line of best fit b) superimposed ΔE^*_{ab} results of specimen Anaconda EPR with linear line of best fit c) shift factor of superimposed Anaconda EPR ΔE^*_{ab} results plotted against temperature used to calculate E_a d) plotted average ΔE^*_{ab} as a function of aging temperature and duration for specimen Rockbestos XLPE with a linear line of best fit e) superimposed ΔE^*_{ab} results of specimen Rockbestos XLPE with linear line of best fit f) shift factor of superimposed Rockbestos XLPE ΔE^*_{ab} results plotted against temperature used to calculate E_a g) plotted average ΔE^*_{ab} as a function of aging temperature and duration for specimen Brand Rex XLPE with a linear line of best fit h) superimposed ΔE^*_{ab} results of specimen Brand Rex XLPE with linear line of best fit i) shift factor of superimposed Brand Rex XLPE ΔE^*_{ab} results plotted against temperature used to calculate E_a.

Table A4. E_a as calculated from ΔE^*_{ab} at the center and edge (n = 0.95) of investigated specimens.

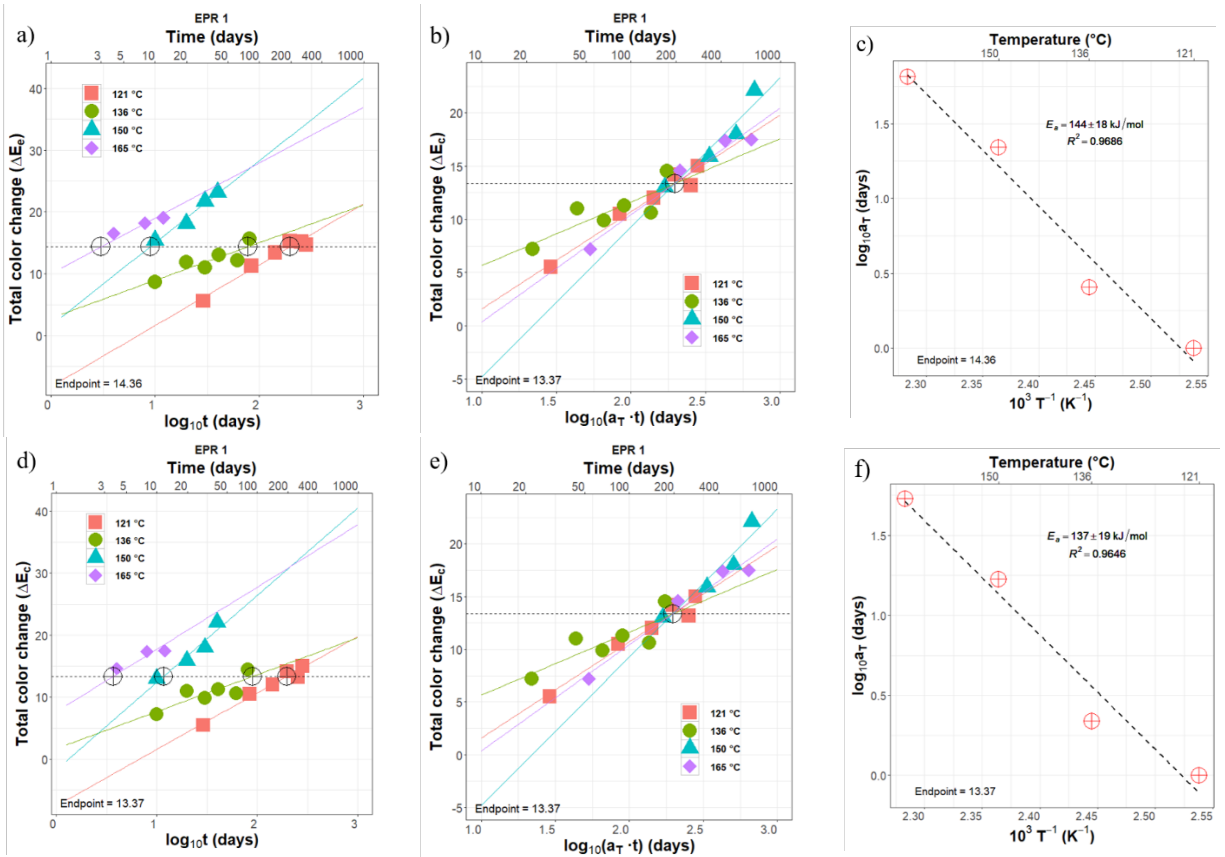| Materials	E_a (kJ/mol)			
	Exterior edge (n = 0.95)	R^2	Center (n = 0.5)	R^2
Anaconda EPR	144 ± 18	0.969	137 ± 19	0.965
Rockbestos XLPE	25 ± 51	0.195	14 ± 34	0.149
Brand Rex XLPE	217 ± 17	0.987	192 ± 5	0.999

Figure A10. a) plotted ΔE^*_{ab} from specimen edge (n = 0.95) as a function of aging temperature and duration for specimen Anaconda EPR with a linear line of best fit b) superimposed ΔE^*_{ab} results from specimen edge of Anaconda EPR with linear line of best fit c) shift factor of superimposed Anaconda EPR ΔE^*_{ab} results from the specimen edge plotted against temperature used to calculate E_a d) plotted ΔE^*_{ab} from specimen center (n = 0.5) as a function of aging temperature and duration for specimen Anaconda EPR with a linear line of best fit e) superimposed ΔE^*_{ab} results from specimen center of Anaconda EPR with linear line of best fit f) shift factor of superimposed Anaconda EPR ΔE^*_{ab} results from the specimen center plotted against temperature used to calculate E_a.
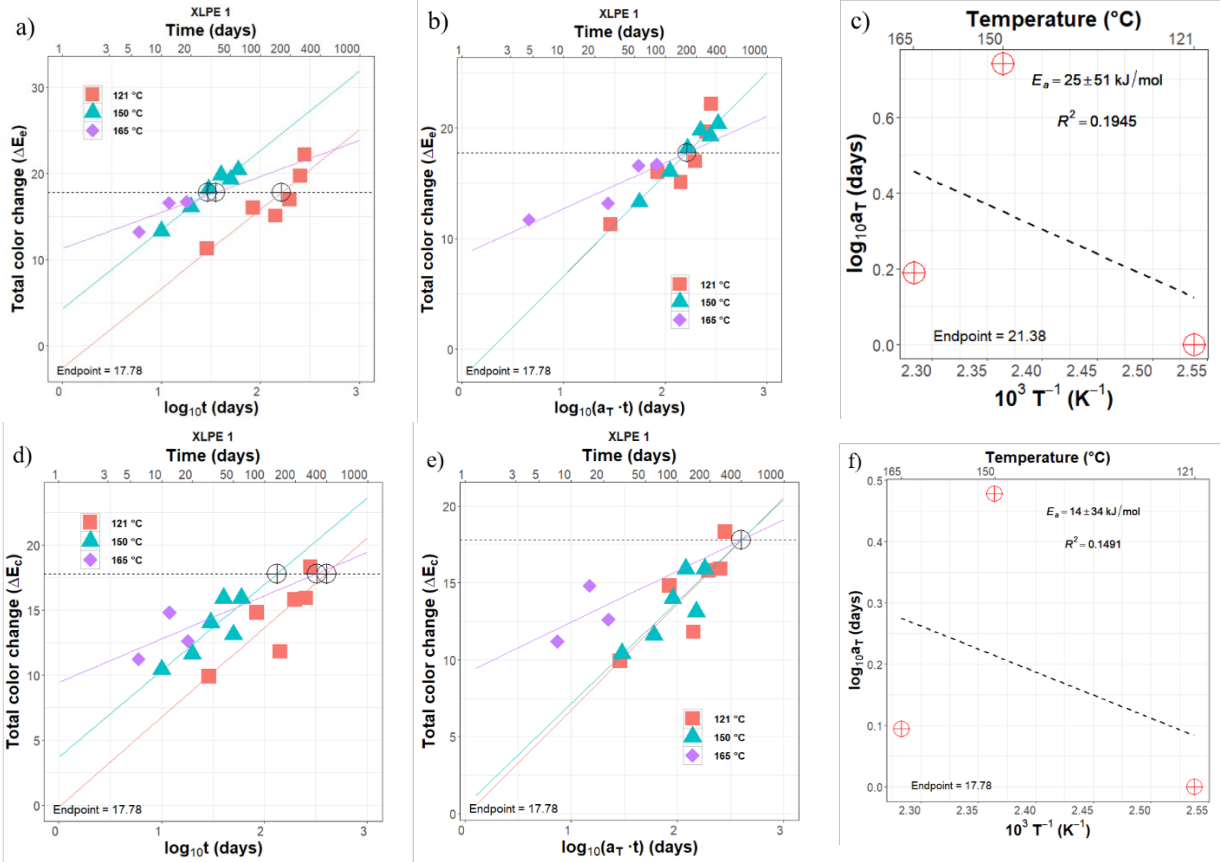
Figure A11. a) plotted ΔE^*_{ab} from specimen edge (n = 0.95) as a function of aging temperature and duration for specimen Rockbestos XLPE with a linear line of best fit b) superimposed ΔE^*_{ab} results from specimen edge of Rockbestos XLPE with linear line of best fit c) shift factor of superimposed Rockbestos XLPE ΔE^*_{ab} results from the specimen edge plotted against temperature used to calculate E_a d) plotted ΔE^*_{ab} from specimen center (n = 0.5) as a function of aging temperature and duration for specimen Rockbestos XLPE with a linear line of best fit e) superimposed ΔE^*_{ab} results from specimen center of Rockbestos XLPE with linear line of best fit f) shift factor of superimposed Rockbestos XLPE ΔE^*_{ab} results from the specimen center plotted against temperature used to calculate E_a.
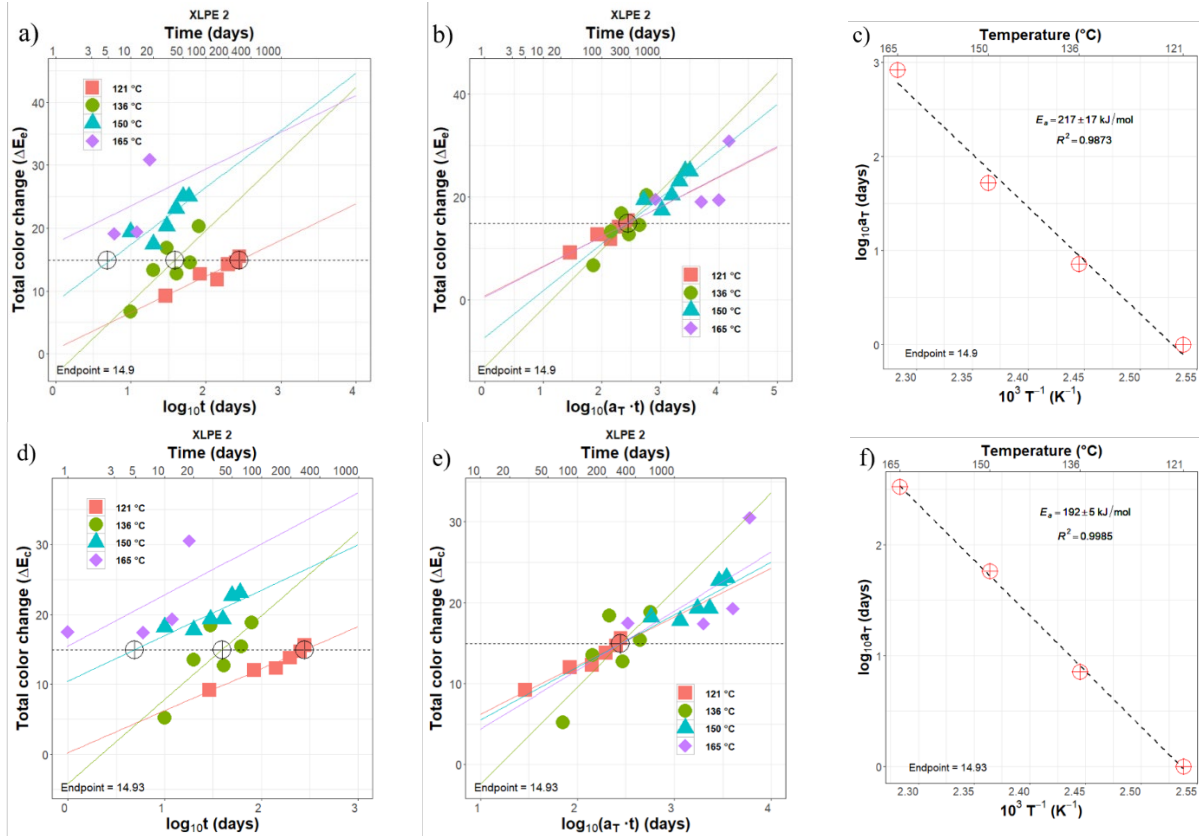
Figure A12. a) plotted ΔE^*_{ab} from specimen edge (n = 0.95) as a function of aging temperature and duration for specimen Brand Rex XLPE with a linear line of best fit b) superimposed ΔE^*_{ab} results from specimen edge of Brand Rex XLPE with linear line of best fit c) shift factor of superimposed Brand Rex XLPE ΔE^*_{ab} results from the specimen edge plotted against temperature used to calculate E_a d) plotted ΔE^*_{ab} from specimen center (n = 0.5) as a function of aging temperature and duration for specimen Brand Rex XLPE with a linear line of best fit e) superimposed ΔE^*_{ab} results from specimen center of Brand Rex XLPE with linear line of best fit f) shift factor of superimposed Brand Rex XLPE ΔE^*_{ab} results from the specimen center plotted against temperature used to calculate E_a.

Table A5. Calculated activation energies from EAB results using high and low temperatures.

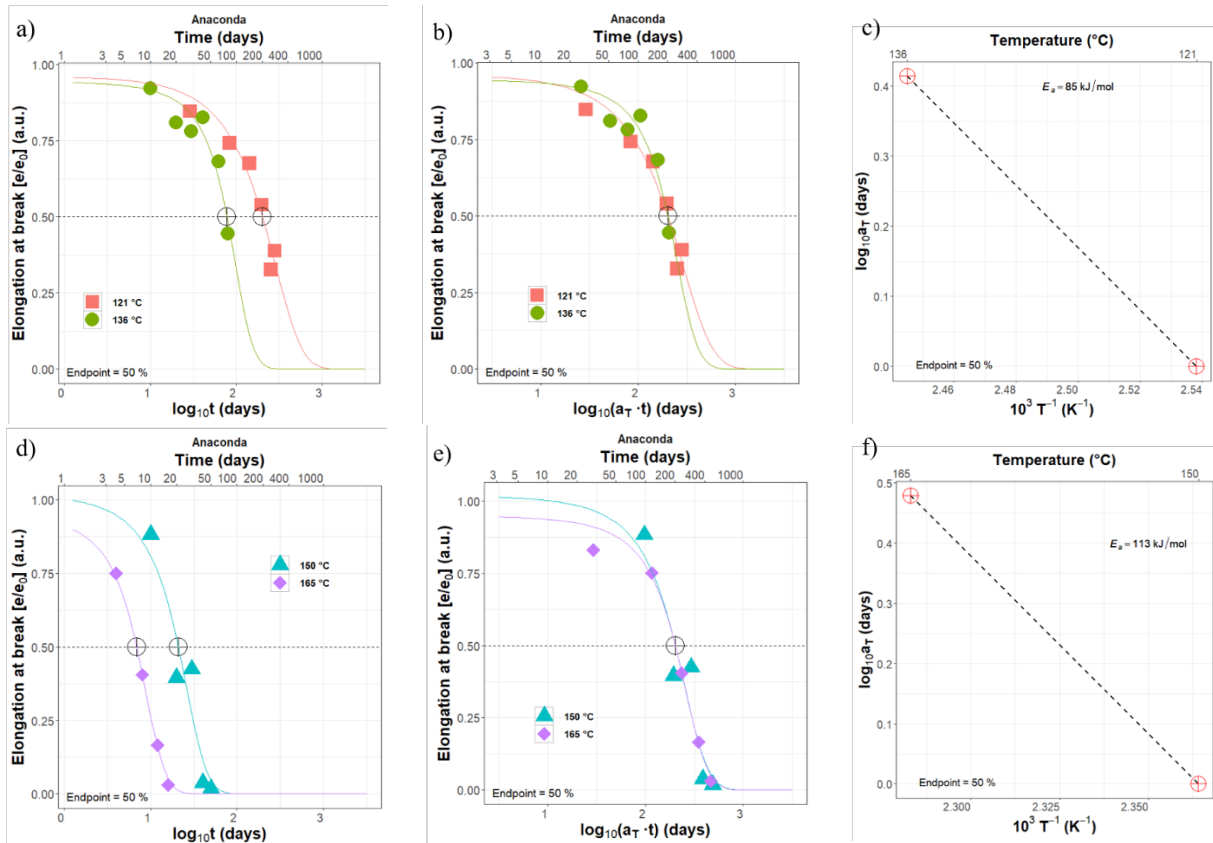| Specimen ID	E_a (kJ/mol)	Isothermal curves used
Anaconda EPR	85	136 °C & 121 °C
	113	165 °C & 150 °C
Rockbestos XLPE	63	150 °C & 121 °C
	143	165 °C & 150 °C
Brand Rex XLPE	113	136 °C & 121 °C
	153	165 °C & 150 °C

Figure A13. a) plotted EAB results of specimen Anaconda EPR aged at lower temperatures (121 °C – 136 °C) with sigmoidal line of best fit b) superimposed EAB results of specimen Anaconda EPR aged at lower temperatures (121 °C – 136 °C) with sigmoidal line of best fit c) shift factor of superimposed Anaconda EPR EAB results aged at lower temperatures (121 °C – 136 °C) plotted against temperature used to calculate E_a d) plotted EAB results of specimen Anaconda EPR aged at higher temperatures (150 °C – 165 °C) with sigmoidal line of best fit e) superimposed EAB results of specimen Anaconda EPR aged at higher temperatures (150 °C – 165 °C) with sigmoidal line of best fit f) shift factor of superimposed Anaconda EPR EAB results aged at higher temperatures (150 °C – 165 °C) plotted against temperature used to calculate E_a.
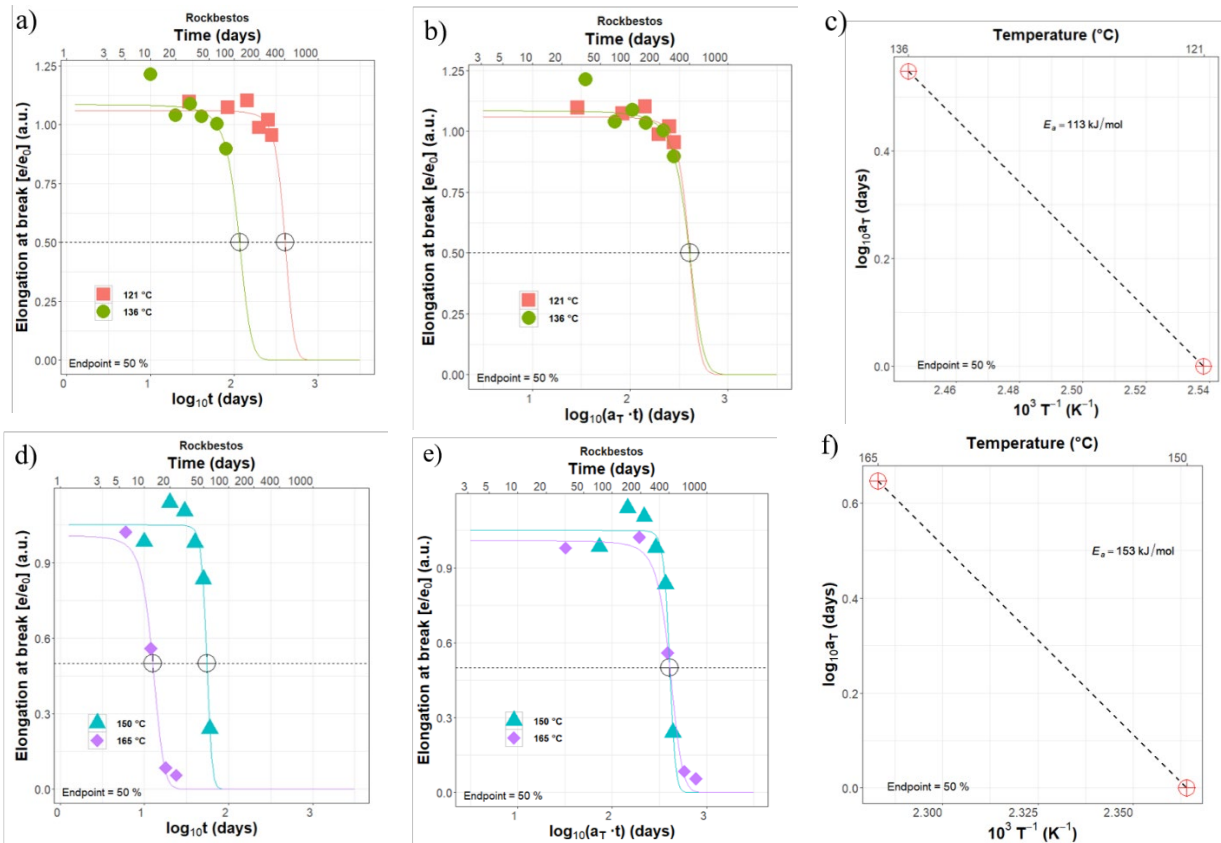
Figure A14. a) plotted EAB results of specimen Rockbestos XLPE aged at lower temperatures (121 °C – 136 °C) with sigmoidal line of best fit b) superimposed EAB results of specimen Rockbestos XLPE aged at lower temperatures (121 °C – 136 °C) with sigmoidal line of best fit c) shift factor of superimposed Rockbestos XLPE EAB results aged at lower temperatures (121 °C – 136 °C) plotted against temperature used to calculate E_a d) plotted EAB results of specimen Rockbestos XLPE aged at higher temperatures (150 °C – 165 °C) with sigmoidal line of best fit e) superimposed EAB results of specimen Rockbestos XLPE aged at higher temperatures (150 °C – 165 °C) with sigmoidal line of best fit f) shift factor of superimposed Rockbestos XLPE EAB results aged at higher temperatures (150 °C – 165 °C) plotted against temperature used to calculate E_a.
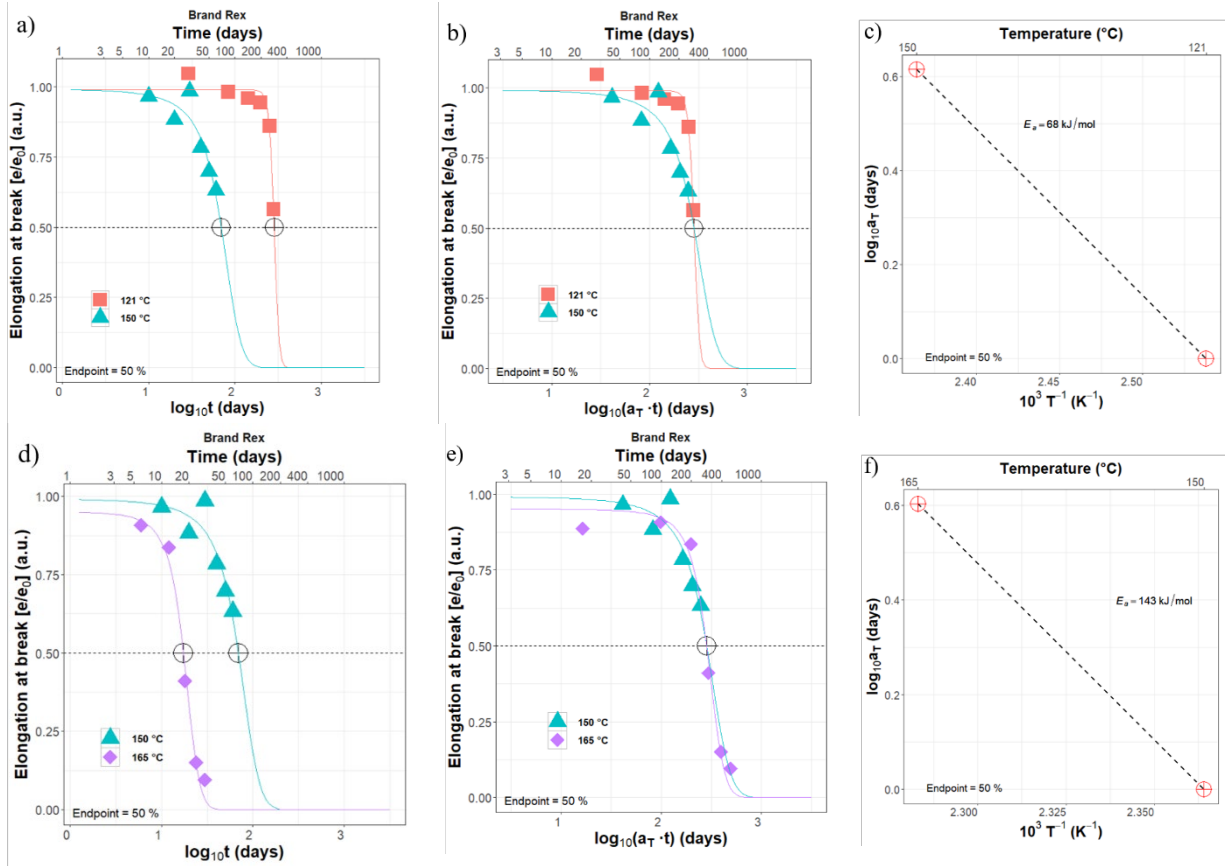
Figure A15. a) plotted EAB results of specimen Brand Rex XLPE aged at lower temperatures (121 °C – 150 °C) with sigmoidal line of best fit b) superimposed EAB results of specimen Brand Rex XLPE aged at lower temperatures (121 °C – 150 °C) with sigmoidal line of best fit c) shift factor of superimposed Brand Rex XLPE EAB results aged at lower temperatures (121 °C – 150 °C) plotted against temperature used to calculate E_a d) plotted EAB results of specimen Brand Rex XLPE aged at higher temperatures (150 °C – 165 °C) with sigmoidal line of best fit e) superimposed EAB results of specimen Brand Rex XLPE aged at higher temperatures (150 °C – 165 °C) with sigmoidal line of best fit f) shift factor of superimposed Brand Rex XLPE EAB results aged at higher temperatures (150 °C – 165 °C) plotted against temperature used to calculate E_a.